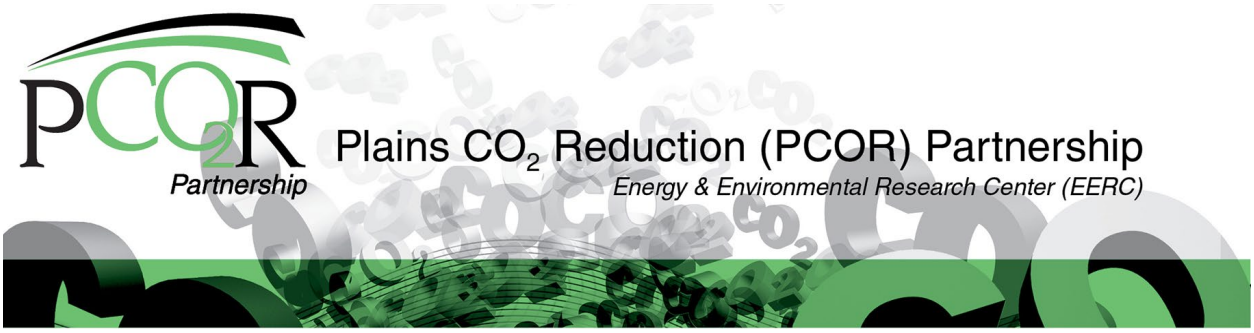

NATIONAL RISK ASSESSMENT PARTNERSHIP (NRAP) TESTING AND VALIDATION: PART 1 – NRAP OPEN-SOURCE INTEGRATED ASSESSMENT MODEL (OPEN-IAM)

Plains CO_2 Reduction (PCOR) Partnership
Task 3 – Deliverable D10 – Part 1

Prepared for:

Joshua Hull

National Energy Technology Laboratory
U.S. Department of Energy
626 Cochrans Mill Road
PO Box 10940
Pittsburgh, PA 15236-0940

Cooperative Agreement No. DE-FE0031838

Prepared by:

Fazilatun N. Mahmood
Nicholas A. Azzolina
David V. Nakles
Ian K. Feole
Kevin C. Connors

Energy & Environmental Research Center
University of North Dakota
15 North 23rd Street, Stop 9018
Grand Forks, ND 58202-9018

December 2021
Approved January 2023

2023-EERC-01-11

EERC DISCLAIMER

LEGAL NOTICE This research report was prepared by the Energy & Environmental Research Center (EERC), an agency of the University of North Dakota, as an account of work sponsored by the U.S. Department of Energy (DOE). Because of the research nature of the work performed, neither the EERC nor any of its employees makes any warranty, express or implied, or assumes any legal liability or responsibility for the accuracy, completeness, or usefulness of any information, apparatus, product, or process disclosed or represents that its use would not infringe privately owned rights. Reference herein to any specific commercial product, process, or service by trade name, trademark, manufacturer, or otherwise does not necessarily constitute or imply its endorsement or recommendation by the EERC.

ACKNOWLEDGMENT

This material is based upon work supported by DOE's National Energy Technology Laboratory under Award No. DE-FE0031838 and the North Dakota Industrial Commission (NDIC) under Contract Nos. FX-XCI-226 and G-050-96.

DOE DISCLAIMER

This report was prepared as an account of work sponsored by an agency of the United States Government. Neither the United States Government, nor any agency thereof, nor any of their employees, makes any warranty, express or implied, or assumes any legal liability or responsibility for the accuracy, completeness, or usefulness of any information, apparatus, product, or process disclosed, or represents that its use would not infringe privately owned rights. Reference herein to any specific commercial product, process, or service by trade name, trademark, manufacturer, or otherwise does not necessarily constitute or imply its endorsement, recommendation, or favoring by the United States Government or any agency thereof. The views and opinions of authors expressed herein do not necessarily state or reflect those of the United States Government or any agency thereof.

NDIC DISCLAIMER

This report was prepared by the Energy & Environmental Research Center (EERC) pursuant to an agreement partially funded by the Industrial Commission of North Dakota, and neither the EERC nor any of its subcontractors nor the North Dakota Industrial Commission nor any person acting on behalf of either:

(A) Makes any warranty or representation, express or implied, with respect to the accuracy, completeness, or usefulness of the information contained in this report or that the use of any information, apparatus, method, or process disclosed in this report may not infringe privately owned rights; or

(B) Assumes any liabilities with respect to the use of, or for damages resulting from the use of, any information, apparatus, method, or process disclosed in this report.

Reference herein to any specific commercial product, process, or service by trade name, trademark, manufacturer, or otherwise does not necessarily constitute or imply its endorsement, recommendation, or favoring by the North Dakota Industrial Commission. The views and opinions of authors expressed herein do not necessarily state or reflect those of the North Dakota Industrial Commission.

TABLE OF CONTENTS

LIST OF FIGURES

Continued . . .

LIST OF FIGURES (continued)

Continued . . .

LIST OF FIGURES (continued)

LIST OF TABLES

NATIONAL RISK ASSESSMENT PARTNERSHIP (NRAP) TESTING AND VALIDATION: PART 1 – NRAP OPEN-SOURCE INTEGRATED ASSESSMENT MODEL (OPEN-IAM)

EXECUTIVE SUMMARY

The Energy & Environmental Research Center tested and validated the National Risk Assessment Partnership (NRAP) Open-source Integrated Assessment Model (Open-IAM). This report presents the results of these efforts, which were conducted under Subtask 3.2 (NRAP Validation) of Task 3 (Data Collection, Sharing, and Analysis) of the Plains CO_2 Reduction Partnership Initiative to Accelerate Carbon Capture, Utilization, and Storage Deployment (hereafter "PCOR Partnership Initiative").

The NRAP testing and validation plans of the PCOR initiative currently include two NRAP tools: i) Open-IAM and ii) Designs for Risk Evaluation and Management (DREAM). The testing and validation of these tools are intended to support their ongoing development. In particular, the testing is assessing the ability of the Open-IAM and DREAM tools to support decision-making for a CO_2 storage project considering compliance with the Safe Drinking Water Act requirements, which include provisions for the Underground Injection Control Program of the U.S. Environmental Protection Agency (Class VI Rule of the UIC Program) and North Dakota Administrative Code Sections 43-05-01-01 to 43-05-01-20. The testing outputs for each tool will be summarized in a report that documents the specific version of the tool, input files and assumptions, output files, and recommendations for improving the tool. This Open-IAM testing summary report is Part 1 of 2 of Deliverable D10 (NRAP Testing and Validation). A second summary report (Part 2 of 2 of Deliverable D10) specific to DREAM will be prepared at a later date. These summary reports for each tool will be consolidated into a single report, Deliverable D10.

The Open-IAM version alpha 2.2.0-21.02.12, which required installation of Python version 3.7.6-amd64, was tested. It incorporated a generalized stratigraphy of the primary hydrostratigraphic units for the Williston Basin, North Dakota, and reservoir simulations of pressure and CO_2 saturation designed to reflect a clastic shelf depositional environment with four CO_2 injection wells and a target CO_2 mass injection rate of 4 million metric tons of CO_2 per year. Six Open-IAM components were included in the test program: **i) Model Component:** outlines model parameters that include simulation name, end time, time step, types of simulation and/or analysis, and output directory; **ii) Stratigraphy Component:** defines the stratigraphy of the storage complex that includes the thickness of the storage reservoir and overlying hydrostratigraphic units; **iii) Lookup Table Reservoir Component:** consists of a reduced-order model (ROM), which is based on the interpolation of inputs from a set of lookup tables that are

created from the reservoir simulation results for pressure and CO_2 saturation; **iv) Multisegmented Wellbore Component:** allows the Open-IAM to assign multiple hypothetical leaky wells as potential vertical leakage pathways that connect the storage reservoir to the overlying aquifers in the storage complex; **v) FutureGen 2.0 Above Zone Monitoring Interval (AZMI) Component:** consists of a ROM, which is recommended for aquifers with depths ranging from 700 to 1600 m and an aquifer thickness ranging from 30 to 90 m, that models the dissipation interval between the storage reservoir and the lowermost underground source of drinking water (USDW) and predicts the size of "impact plumes" according to five metrics (pH, total dissolved solids [TDS], pressure, dissolved CO_2, and temperature) and defines their volume (m^3) and dimensions (m) in the *x*- (length), *y*- (width), and *z*-direction (height); and **vi) FutureGen 2.0 Aquifer Component:** consists of a ROM, which is recommended for aquifers with depths ranging from 100 to 700 m and an aquifer thickness ranging from 30 to 90 m, that models the USDW and predicts the size of "impact plumes" according to four metrics: pH, TDS, pressure, and dissolved CO_2.

This report provides step-by-step instructions and input files for reproducing the Open-IAM testing, summarizes the Open-IAM simulation results for brine and CO_2 leakage, and presents key findings to support the ongoing development of the Open-IAM.

The test results showed that the current version of Open-IAM is a useful tool for the heuristic modeling of a storage project and what-if scenario modeling for brine and CO_2 leakage through wellbores. However, the current tool requires significant experience with the Open-IAM graphical user interface (GUI) and component modules and may not be easily used by nonexperts. Improvements in the ability to transfer simulations more easily from a numerical reservoir simulator to Open-IAM and the GUI input fields would likely broaden the usability of Open-IAM to a wider set of potential users, for example, regulatory stakeholders.

NATIONAL RISK ASSESSMENT PARTNERSHIP (NRAP) TESTING AND VALIDATION: PART 1 – NRAP OPEN-SOURCE INTEGRATED ASSESSMENT MODEL (OPEN-IAM)

INTRODUCTION

The Plains CO_2 Reduction (PCOR) Partnership Initiative is one of four projects operating under the U.S. Department of Energy (DOE) National Energy Technology Laboratory (NETL) Regional Initiative to Accelerate CCUS (carbon capture, utilization, and storage). The PCOR Partnership Initiative region encompasses ten U.S. states and four Canadian provinces in the upper Great Plains and northwestern regions of North America. The PCOR Partnership Initiative is led by the Energy & Environmental Research Center (EERC) with support from the University of Wyoming and the University of Alaska Fairbanks and includes stakeholders from the public and private sectors. The goal of this joint government–industry effort is to identify and address regional capture, transport, use, and storage challenges facing commercial deployment of CCUS throughout the PCOR Partnership region.

Task 3 (Data Collection, Sharing, and Analysis) of the PCOR Partnership Initiative includes Subtask 3.2 (NRAP Validation) for assessing several National Risk Assessment Partnership (NRAP) tools that evaluate risk proxies for geologic CO_2 sequestration projects (storage projects). Two NRAP tools are currently the focus of the planned Subtask 3.2 testing: i) NRAP open-source integrated assessment model (Open-IAM) (Vasylkivska and others, 2021) and ii) designs for risk evaluation and management (DREAM) (Yonkofski and others, 2020). The testing of these NRAP tools is intended to support their ongoing development and validation. In particular, the testing is assessing the performance of the Open-IAM and DREAM tools to support decision-making for a storage project considering both compliance with the Safe Drinking Water Act requirements as well as provisions for the Underground Injection Control (UIC) Program of the U.S. Environmental Protection Agency (EPA) (Class VI Rule of the UIC Program) and North Dakota Administrative Code Sections 43-05-01-01 to 43-05-01-20. The output of the testing for each tool is a summary report that documents the specific version of the tool, input files and assumptions, output files, and recommendations for improving the tool. These summary reports for each tool will be consolidated into a single report in Deliverable (D) 10 (NRAP Testing and Validation). This document is Part 1 of 2 of D10 and is specific to the Open-IAM. A second document (Part 2 of 2 of D10) specific to DREAM will be prepared later.

Open-IAM is an open-source integrated assessment model developed as part of the NRAP Phase II research to facilitate quantitative risk assessment, management, and containment assurance for storage projects (Vasylkivska and others, 2021). The current version of Open-IAM

(alpha 2.2.0-21.02.12) is in active development and is available for testing and feedback. Open-IAM allows the user to define a conceptual model for a storge complex—a subsurface geologic system comprising a storage unit and primary and, possibly, secondary seal(s), extending laterally to the defined limits of the CO_2 storage operation or operations (Canadian Standards Association, 2012; International Organization for Standardization, 2017)—and to simulate leakage of CO_2 or displaced formation fluids (brine) via leaky wellbores from the storage unit to overlying aquifers or the atmosphere. Therefore, Open-IAM provides a quantitative modeling tool to support risk management decisions for storage projects.

The Open-IAM testing used outputs from a numerical reservoir simulation conducted in Computer Modelling Group's compositional simulator, GEM (CMG GEM). These reservoir simulations were generated as part of a suite of simulations for Task 4 (Real-Time Forecasting and History-Matching) of DOE's SMART-CS (Science-informed Machine Learning for Accelerating Real-Time Decisions in Subsurface Applications Initiative under the Carbon Storage) Program. The simulation results used for the Open-IAM testing represented a generic storage complex that was designed to reflect a clastic shelf depositional environment with four CO_2 injection wells and a target CO_2 mass injection rate of 4 million metric tons of CO_2 per year ($MtCO_2$/year). These simulation results were exported from CMG GEM, imported into PETREL, and exported as a Gslib (Geostat Library) output file for use in Open-IAM. Customized postprocessing in Python was used to convert the Gslib output into a format that could be imported into the current version of Open-IAM. The Open-IAM testing evaluated hypothetical leakage scenarios of CO_2 and brine from the storage reservoir, up a set of hypothetical leaky wellbores, and into the lowermost underground source of drinking water (USDW). In addition, the Open-IAM testing included an examination of the effect of a "thief zone" – an intermediary saline aquifer between the primary seal (cap rock) and USDW – on the leakage rate to the USDW. The loss of fluid into this thief zone lowers the vertical hydraulic head gradient with increasing vertical location in a leaky wellbore, thereby decreasing vertical fluid migration above the saline aquifer to the USDW (Nordbotten et al., 2004). The hypothetical leakage scenarios explored different input assumptions about the properties of the hypothetical leaky wellbores and thief zone aquifer. The remainder of this document discusses the Open-IAM installation, operation, and results of the testing.

INSTALLING OPEN-IAM

The testing used Open-IAM version alpha 2.2.0-21.02.12, which required installation of Python version 3.7.6-amd64. Open-IAM was downloaded from a public GitLab repository located at https://gitlab.com/NRAP/OpenIAM/-/tree/a2.2.0. The installation instructions found in the file "Installation_Instructions_Windows.txt" (https://gitlab.com/NRAP/OpenIAM/-/tree/a2.2.0/installers/Windows_10) provided step-by-step instructions for installing Anaconda and Python and downloading and testing Open-IAM (Figure 1). The installation instruction file recommended installing Anaconda because Anaconda provides easily accessible functionality to different versions of Python and works as an interface to manage different existing Python environments without interruption. Since Python was installed through Anaconda, the Anaconda prompt was used for the setup and testing of Open-IAM instead of the command prompt. The Open-IAM tool

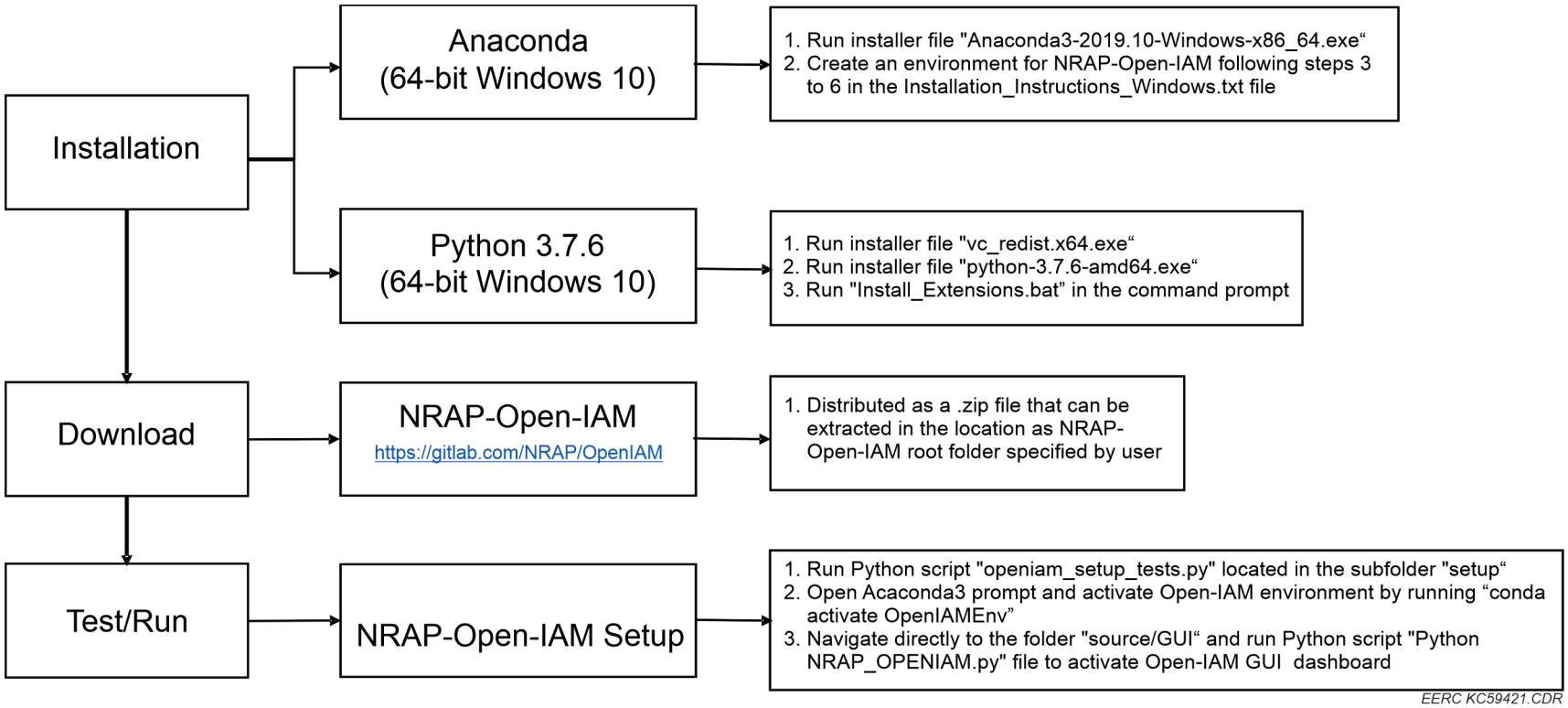

Figure 1. Workflow illustrating the processes of installation, download, and test/run of the NRAP-Open-IAM.

and examples were downloaded as a .zip file from the public GitLab repository. The contents of the .zip file were then extracted and saved to a local directory specified by the user. Open-IAM provided several options to build and run simulations that include a graphical user interface (GUI), control files, and Python scripts. The testing was conducted using the GUI to build and run scenarios in the Open-IAM.

OPEN-IAM GUI OPERATION

The Open-IAM GUI was launched using the Anaconda prompt by running the Python script "Python NRAP_OPENIAM.py" located in the Open-IAM root folder (e.g., C:\OpenIAM-master (alpha 2.2.0)\source\GUI), which brings the user to the Open-IAM Main Page.

The Open-IAM Main Page has three primary buttons at the top of the page: Enter Parameters, Load Simulation, and Post Processing. The Enter Parameters button is used to create an initial set of inputs for an Open-IAM simulation. The Load Simulation button allows the user to open an existing Open-IAM simulation file. The Post Processing button allows the user to conduct postprocessing and/or plotting of results of the Open-IAM simulations.[1] Since the testing required the creation of an initial set of inputs, it began with the Enter Parameters button.

Enter Parameters

The Enter Parameters button is used to create an initial set of inputs for an Open-IAM simulation (Figure 2). Selecting the Enter Parameters button takes the user to a set of Open-IAM components. Open-IAM is an "integrated assessment model" in the sense that it integrates outputs from different components under a single tool. While the current version of Open-IAM includes 14 different components, the testing conducted herein utilized only six components: Model Parameters, Stratigraphy, Lookup Table Reservoir, Multisegmented Wellbore, FutureGen 2.0 AZMI (Above Zone Monitoring Interval), and FutureGen 2.0 Aquifer.

Each component allows the user to enter component-specific parameters and input files (comma-separated values [.csv] files). The general process for creating the initial set of inputs for an Open-IAM simulation using these components starts with i) [Model Component] Outline model parameters that include simulation name, end time, time step, types of simulation and/or analysis, and output directory; ii) [Stratigraphy Component] Define the stratigraphy of the storage complex that includes the thickness of the storage reservoir and overlying hydrostratigraphic units, and iii) Assign the additional model components for the system: [Lookup Table Reservoir Component], [Multisegmented Wellbore Component], [FutureGen 2.0 AZMI Component], and [FutureGen 2.0 Aquifer Component]. Each of these components is described in greater detail below.

[1] Note: The term "simulation" in this context does not refer to the CMG GEM reservoir simulation, which is an input to the Open-IAM. Instead, an Open-IAM simulation refers to the calculations done within the Open-IAM tool to generate the results of the hypothetical leakage scenarios from a set of user-defined inputs.

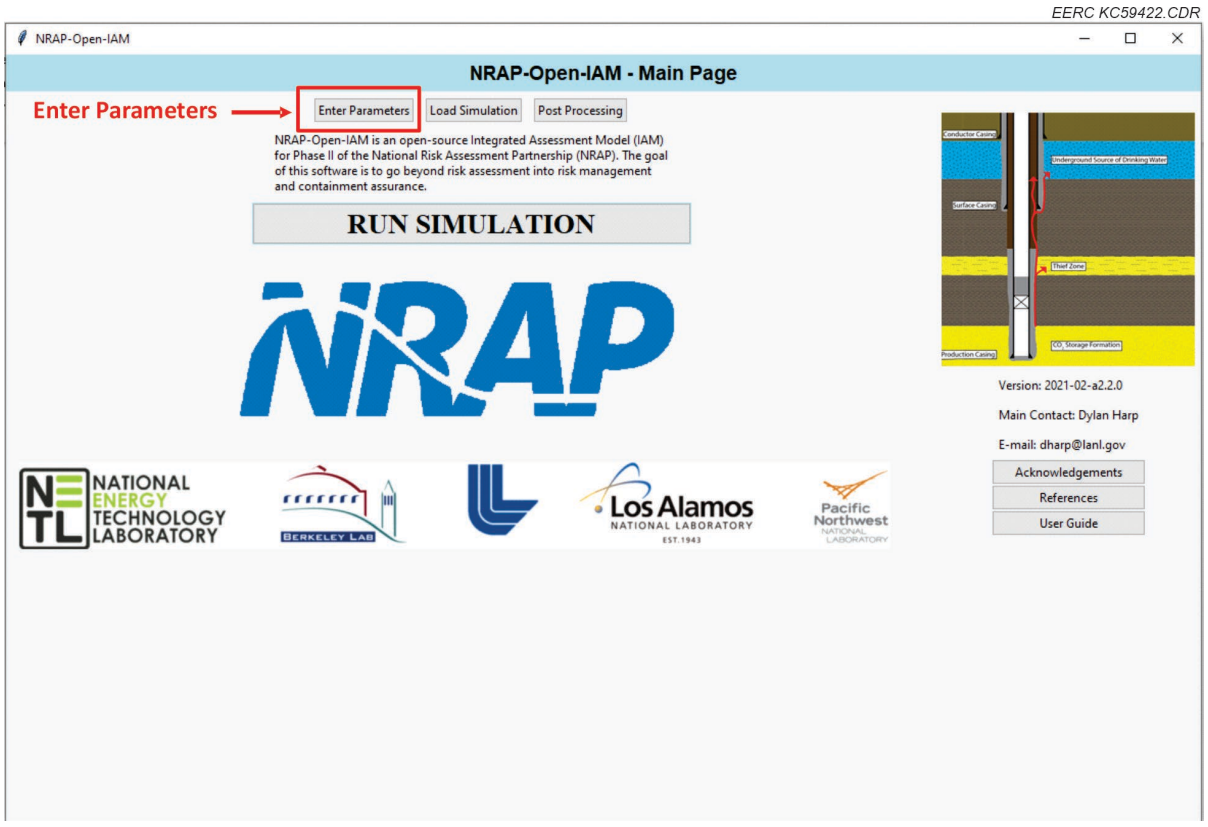

Figure 2. GUI of the NRAP-Open-IAM Main Page showing the selection of the Enter Parameters button (red rectangle), which allows the user to create an initial set of inputs for an Open-IAM simulation.

Model Component

The first step for creating an initial set of inputs for an Open-IAM simulation is to specify model parameters using the Model Component (Figure 3). For file management and version control, each Open-IAM simulation can have a unique "Simulation name." The example simulation name shown here was "OpenIAMTesting_SMART_ClasticShelf_P50-1."

The next set of inputs in the Model Component are "End Time (years)" and "Time Step (years)." The end time is the total number of years to be evaluated, and the time step is a uniform time increment from the start of CO_2 injection until the End Time. The Open-IAM testing was evaluated for a period of 25 years with a 1-year time step (Figure 3), which corresponds to the CMG GEM simulation output files for the operational phase (CO_2 injection period) of the generic storage complex.

The Model Component allows the user to select from three types of analyses: i) Forward, ii) LHS (Latin Hypercube Sampling), and iii) Parstudy (Parameter Study Analysis). Forward analysis runs a single deterministic scenario with fixed input parameters. While the Forward

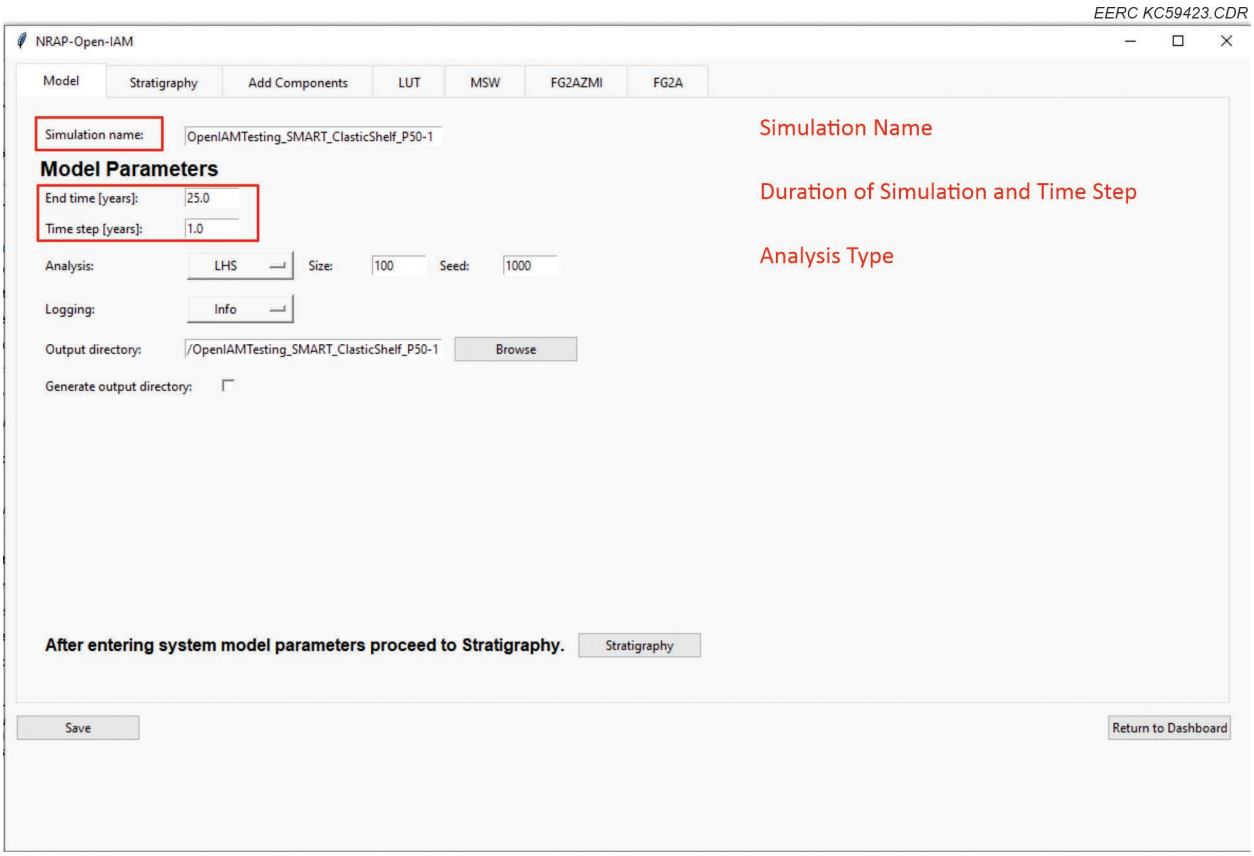

Figure 3. Inputs used in the Model Component for the Open-IAM testing.

analysis provides rapid results and allows the user to quickly answer "what-if" questions about potential leakage scenarios, the Forward analysis does not allow the user to easily evaluate the effect of uncertainty about the input parameters on the Open-IAM outputs. Parstudy divides a user-defined range for each stochastic variable into equally spaced subdomains and selects a parameter value from each subdomain; however, the number of realizations increases exponentially with the number of variables. LHS was selected for this Open-IAM testing because it allows probabilistic parameter sampling to run stochastic simulations, and the number of realizations can be limited by the user to reduce the computational burden and expedite assessments (Figure 3). The benefit of applying a stochastic model with LHS rather than a deterministic model in the Forward analysis is that the user can assess multiple realizations of potential leakage scenarios based on a set of uncertain input parameters, which are sampled from a probability distribution defined by the user. The resultant ensemble of realizations provides better information to the user about the effect of input parameter uncertainty on the variation in the Open-IAM simulation results. For the Open-IAM testing, LHS analysis was run using a sample size of 100 realizations to reduce computational and data postprocessing times.

The last three inputs to complete the Model Component are the selection of a Logging setting, the specification of an Output Directory, and the checking of the box for "Generate Output Directory" (Figure 3). As described in the Open-IAM User Manual (Vasylkivska and others, 2021), Open-IAM creates a log file with each simulation run. The level of information being

logged can be set by changing the value of the Logging entry. In general, the default logging setting of "Info" will contain the most useful messages. However, a Debug (debugging) level of Logging will contain more information about component model connections, setup, and calls but will produce very large files and should be avoided for large simulations. The default Logging setting of "Info" was used for all testing (Figure 3).

Stratigraphy Component

The Stratigraphy Component allows the user to specify the thicknesses of each geologic unit in the storage complex, including the storage reservoir, primary seal (cap rock), and overlying aquifers. Figure 4 shows the stratigraphy used for the Open-IAM testing, which followed a generalized sequence stratigraphy of the primary hydrostratigraphic units for the Williston Basin, North Dakota.

The first parameter to enter in the Stratigraphy Component is the number of shale layers. The default number is three and the maximum number of shale layers is 30. The shale units must be separated by an aquifer. For example, if the number of shale layers is set to three, then the Stratigraphy Component requires two aquifers, one between each shale layer (Figure 5).

The stratigraphic layers are numbered from the bottom to the top of the stratigraphy, such that the first shale layer overlying the storage reservoir (i.e., the primary seal or cap rock) is "Shale 1." the aquifer overlying Shale 1 is "Aquifer 1," etc., leading to the uppermost shale layer (Shale 3). Figure 4 shows the stratigraphic units and thicknesses used in the Open-IAM testing.

The Reservoir unit is the storage reservoir. Aquifer 1 is an intermediary saline aquifer between the storage reservoir and USDW, which acts as a "thief zone" because the loss of fluid into this aquifer lowers the vertical hydraulic head gradient above it in a leaky wellbore, thereby decreasing, or nearly eliminating, vertical fluid migration above the saline aquifer to the USDW (Nordbotten et al., 2004). Aquifer 2 represents the lowermost USDW (Figure 4). The USDW is the primary focus of the assessment because the Safe Drinking Water Act requirements and provisions for the Underground Injection Control Program of EPA (Class VI Rule of the UIC Program) and North Dakota Administrative Code Sections 43-05-01-01 to 43-05-01-20 are designed to protect groundwater resources. In addition, a major technical component of permitting a storage project is the delineation of the area of review (AOR). The AOR is defined as the region surrounding the storage project where underground sources of drinking water may be endangered by the injection activity (North Dakota Administrative Code Section 43-05-01-05.1. Area of review and corrective action). Consequently, the potential for leakage of CO_2 or brine to the USDW is the primary focus of the Open-IAM testing.

The Stratigraphy Component allows the user to specify the thicknesses of each unit as a fixed value or to assign them a statistical distribution. Fixed values were used for the unit thicknesses for all Open-IAM testing. Figure 5 shows the Open-IAM Stratigraphy Component populated with the units and thicknesses from Figure 4.

EERC KC59424.CDR

Rock Unit	Depth Top, ft	Depth Top, m	Unit Thickness, ft	Unit Thickness, m	Rock Unit Description
Shale 3 (Quaternary Units)	0	0	779	237	Clays, silt, sand, gravel
Aquifer 2 (USDW)	779	237	213	65	Sandstone, mudstone
Shale 2	992	302	2,100	640	Shales
Aquifer 1 (Thief Zone)	3,091	942	178	54	Sandstone
Shale 1	3,269	996	731	223	Shales, mudstones, siltstones
Storage Unit	4,000	1219	280	85	Coastal eolian dunes overlain by high-energy, shallow marine beach or offshore bar deposits

Figure 4. Generalized storage complex stratigraphy used in the Open-IAM testing.

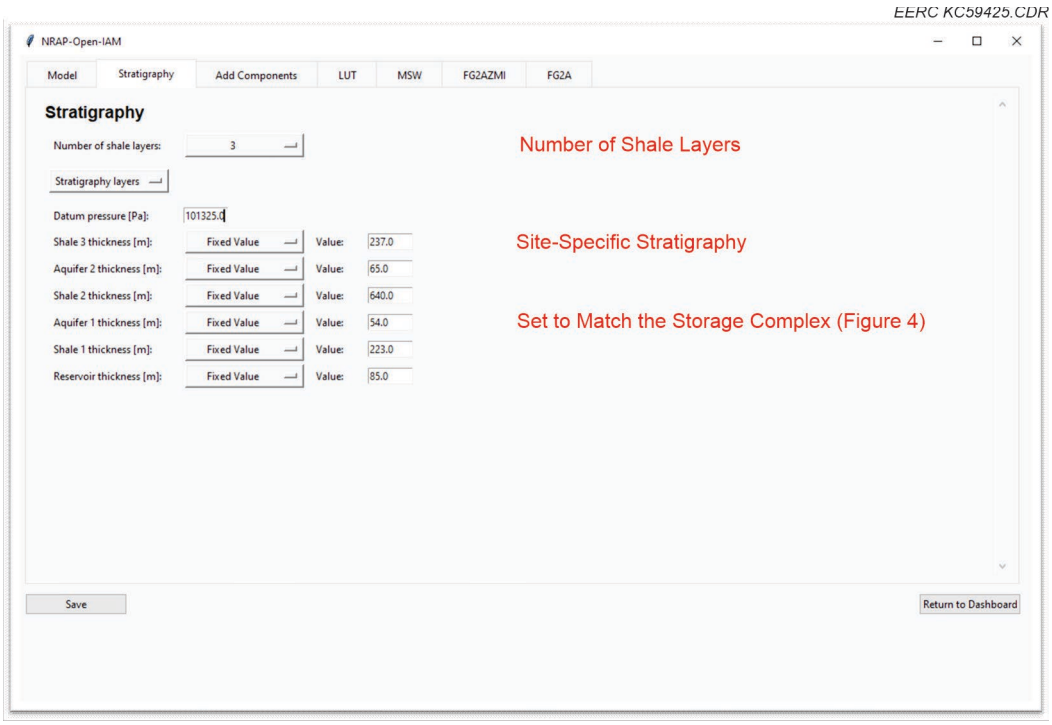

Figure 5. Input parameters used in the Stratigraphy Component for the Open-IAM testing.

Add Components

Beyond specifying the Model Component and Stratigraphy Component inputs, which are common to all Open-IAM simulations, the Add Components feature allows the user to add more components in a sequential order from the deepest component in the stratigraphy upward (e.g., reservoir → wellbore → aquifer) according to the site-specific Open-IAM simulation scenario. As the user specifies a component, a subsequent component can be added and connected to the existing component of the model. For the Open-IAM testing, a Lookup Table (LUT) Reservoir Component was added first, and then a Multisegmented Wellbore (MSW) Component was specified and connected with the LUT Reservoir Component to define the hypothetical leaky wellbores that penetrate the stratigraphy. The FutureGen 2.0 AZMI Component and FutureGen 2.0 Aquifer Component were then connected with the MSW Component to estimate the potential leakage rates of CO_2 and brine from the storage reservoir to the overlying aquifers. This resulted in an Open-IAM simulation that included 1) a site-specific Stratigraphy Component that followed the generalized stratigraphy of the Williston Basin, 2) a LUT Reservoir Component to describe the time-series storage reservoir pressure and CO_2 saturation modeled using CMG GEM, 3) an MSW Component to describe the time-series leakage of CO_2 and brine through a set of hypothetical wellbores placed within the model domain that penetrated the storage reservoir and overlying storage complex, and 4) two Aquifer Components to describe the impacts of CO_2 and brine leakage on Aquifers 1 and 2. Following the addition of all components, the model was saved to return to the Open-IAM Main Page. Additional details about the LUT Reservoir, MSW, FutureGen 2.0 AZMI, and FutureGen 2.0 Aquifer Components are provided in the remainder of this section.

Lookup Table Reservoir Component

The LUT Reservoir Component is a reduced-order model (ROM) based on the interpolation of inputs from a set of LUT created from the CMG GEM reservoir simulation results. The CMG GEM reservoir simulation output must be from a single layer of a three-dimensional (3D) reservoir model, typically near the storage reservoir–cap rock interface or the model layer with the greatest CO_2 plume extent. The CMG GEM reservoir simulation output must include pressure and CO_2 saturation values for each model layer grid cell and Time Step from the start of CO_2 injection to the End Time specified in the Model Component (King, 2016).

The LUT Reservoir Component requires the user to import the following three .csv files (Figure 6):

1. Directory of input files: Named "SMART_layer3_TS25.csv" in the current test. This file contains *x*- and *y*-coordinates of the grid cells (211 × 211) in the first two columns followed by columns of pressure and CO_2 saturation data for each Time Step over the 25-year period.

2. Input time points file: Named "SMART_time_points.csv" in the current test. This file contains time steps (in years) in a single row for the same number of columns for which pressure and CO_2 saturation data are provided in the SMART_layer3_TS25.csv input file.

3. Input parameters file: Named "SMART_parameters_and_filenames.csv" in the current test. This file contains names and values of LUT petrophysical parameters (logResPerm, reservoir Porosity, and logShalePerm) of the CO_2 storage reservoir and shale units.

These three .csv files, "SMART_layer3_TS25.csv," "SMART_time_points.csv," and "SMART_parameters_and_filenames.csv," are included as separate attachments to this report. A notepad entitled "SMART layer3 Hypothetical Wells" is also included as a separate attachment to this report, providing *x*- and *y*-coordinates of each hypothetical leaky wells.

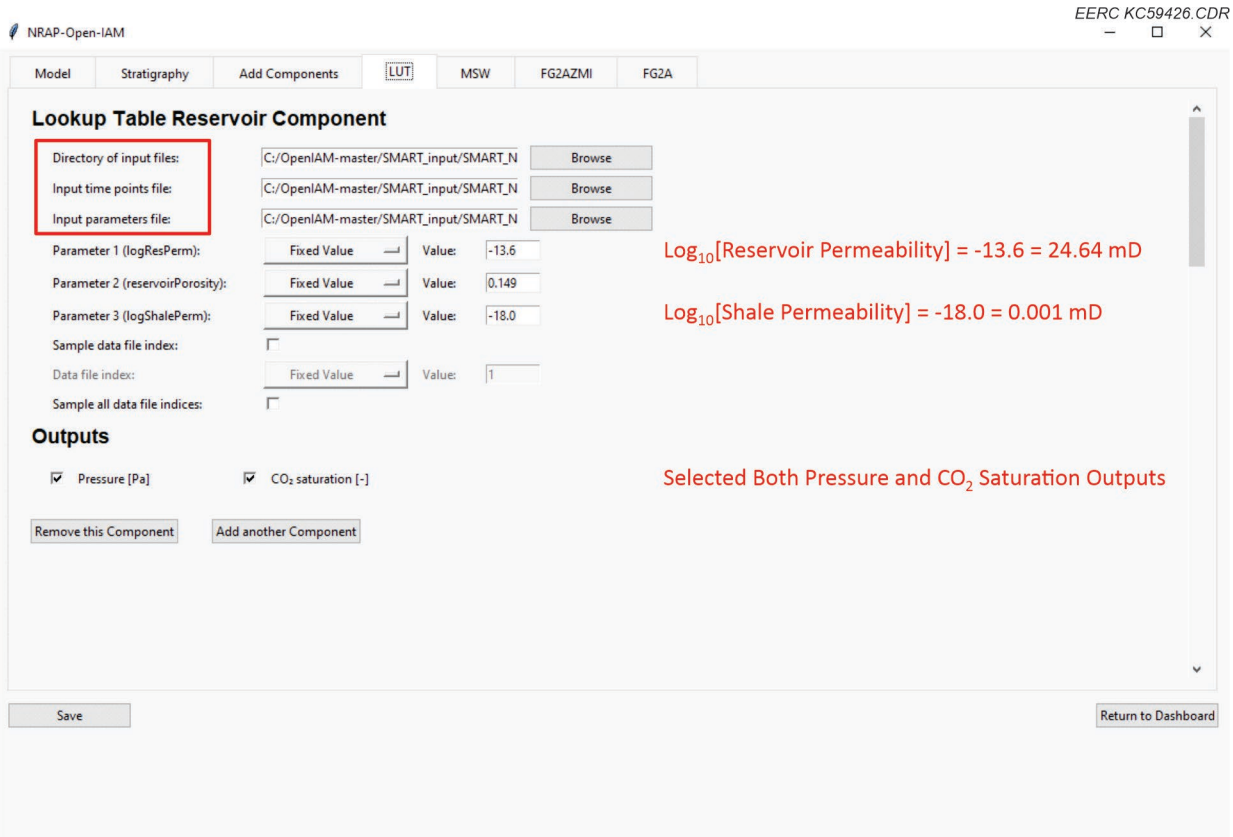

Figure 6. Input files and parameters in the Lookup Table Reservoir Component used for the Open-IAM testing.

The Open-IAM workflow is designed for the input file, time points file, and parameters file to come from CMG GEM simulation results. However, the default export format of the CMG GEM simulation results is not compatible with the input format for the current version of Open-IAM (alpha 2.2.0-21.02.12). Therefore, additional postprocessing was required to restructure the CMG GEM output data format into .csv files. To generate the Open-IAM input file, the CMG GEM simulation results (rescue files containing formation pressure and gas saturation for all model grid cells for all time steps and layers) were imported into Petrel and then exported as a Gslib (Geostat Library)-formatted output file (ASCII). This output file reports the model grid cell index-I, J, and K (Figure 7, Columns A–C), model grid cell center coordinates X, Y, and Z (Figure 7, Columns D–F), and the formation pressure and gas saturation for all storage reservoir layers (K = 1–30) and time steps (t_y = 1–25).

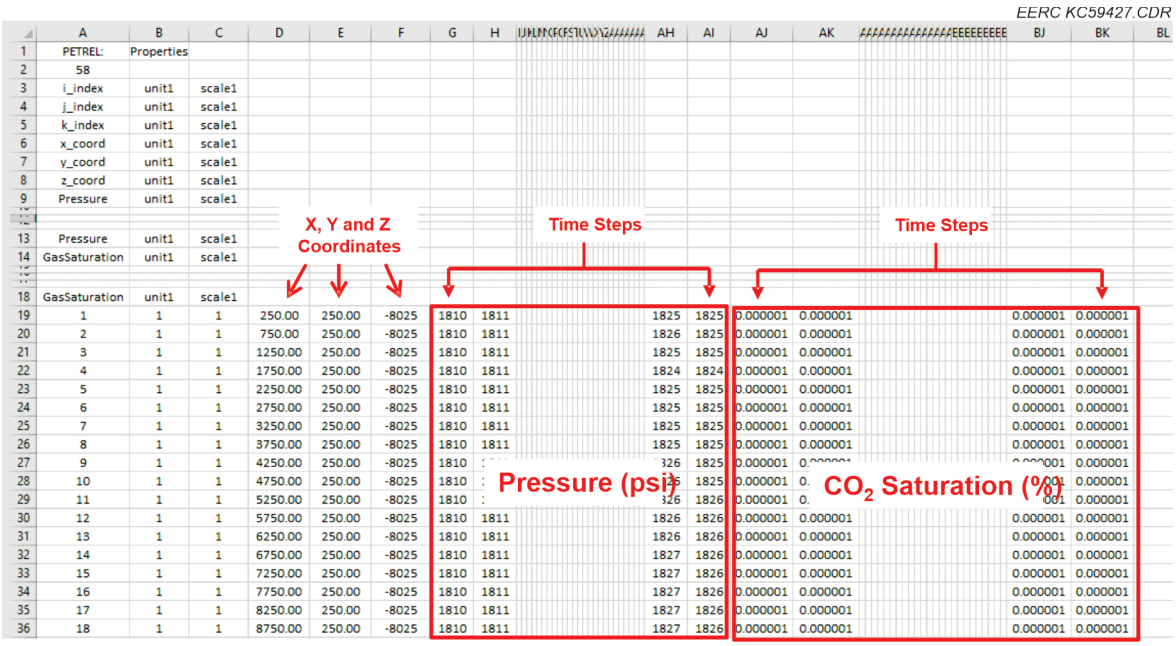

Figure 7. Example of output file exported from PETREL file as a Gslib-formatted output file named "SMART_SgPressure_Layer3" containing formation pressure and gas saturation for all layers and time steps.

A Python script (Figure 8) was written to extract formation pressure and gas saturation for a specific layer (K = 3) of all time steps (t_y = 1–25) from the PETREL-derived Gslib output file into a compatible Open-IAM input .csv file.

Layer K = 3 was chosen for the Open-IAM testing because this layer contained the largest areal extent of CO_2 after 25 years of injection and, therefore, represented the most conservative (i.e., largest) time-series CO_2 plume estimate. Figure 9 shows an example of the Python-reformatted .csv file (SMART_layer3_TS25.csv), which contains *x*- and *y*-coordinates of the 211 × 211 grid cells in the first two columns. The subsequent columns are for pressure data (26 columns from pressure_1 to pressure_26) and CO_2 saturation data (an additional 26 columns from CO2sat_1 to CO2sat_26) corresponding to each Time Step for the 25-year period (including the 0- Time Step).

```
klayer = 3
timesteps = 51
prop = []

with open('sg_pres.out', 'r') as fo:
   for line in fo:
      try:
         if line.split()[2] == "scale1":
            prop.append(line.split()[0])
         if isinstance(float(line.split()[0]),  numbers.Real):
            layers = int(len(prop))
         if len(line.split()) > 3:
            break

      except ValueError:
         pass
      except IndexError:
         pass

fm_index_array = np.loadtxt('sg_pres.out', skiprows=layers+2)
aa = fm_index_array[np.where(fm_index_array[:,2]  == klayer)]
bb = np.delete(aa,  [0, 1, 2, 5], 1)
header = np.delete(prop,[0,  1, 2, 5]).tolist()

sg_header=[]
pres_header=[]

time=0
for x in range(2, timesteps+2):
   time+=1
   sg_header.append(header[x]  + ("_" + str(time)))

time=0
for y in range(53, timesteps*2+2):
   time+=1
   pres_header.append(header[y]  + ("_" + str(time)))

newheader=['x','y']
for z in range(0, len(sg_header)):
   newheader.append(sg_header[z])

for zz in range(0, len(pres_header)):
   newheader.append(pres_header[zz])

gslibProps=['Pressure', 'GasSaturation']

for zzz in range(0, len(newheader)):
   if "Pressure" in newheader[zzz]:
      newheader[zzz]  = newheader[zzz].replace(gslibProps[0],  "pressure")
   elif "GasSaturation" in newheader[zzz]:
      newheader[zzz]  = newheader[zzz].replace(gslibProps[1],  "CO2saturation")

header_str = ",".join(newheader[cc].strip(".csv")  for cc in range(0, len(newheader)))

np.savetxt("sg_pres_layer" + str(klayer) + ".csv", bb, fmt='%.6f', delimiter=',', header=header_str)
```

Figure 8. Python script developed to reformat Petrel-derived Gslib output file.

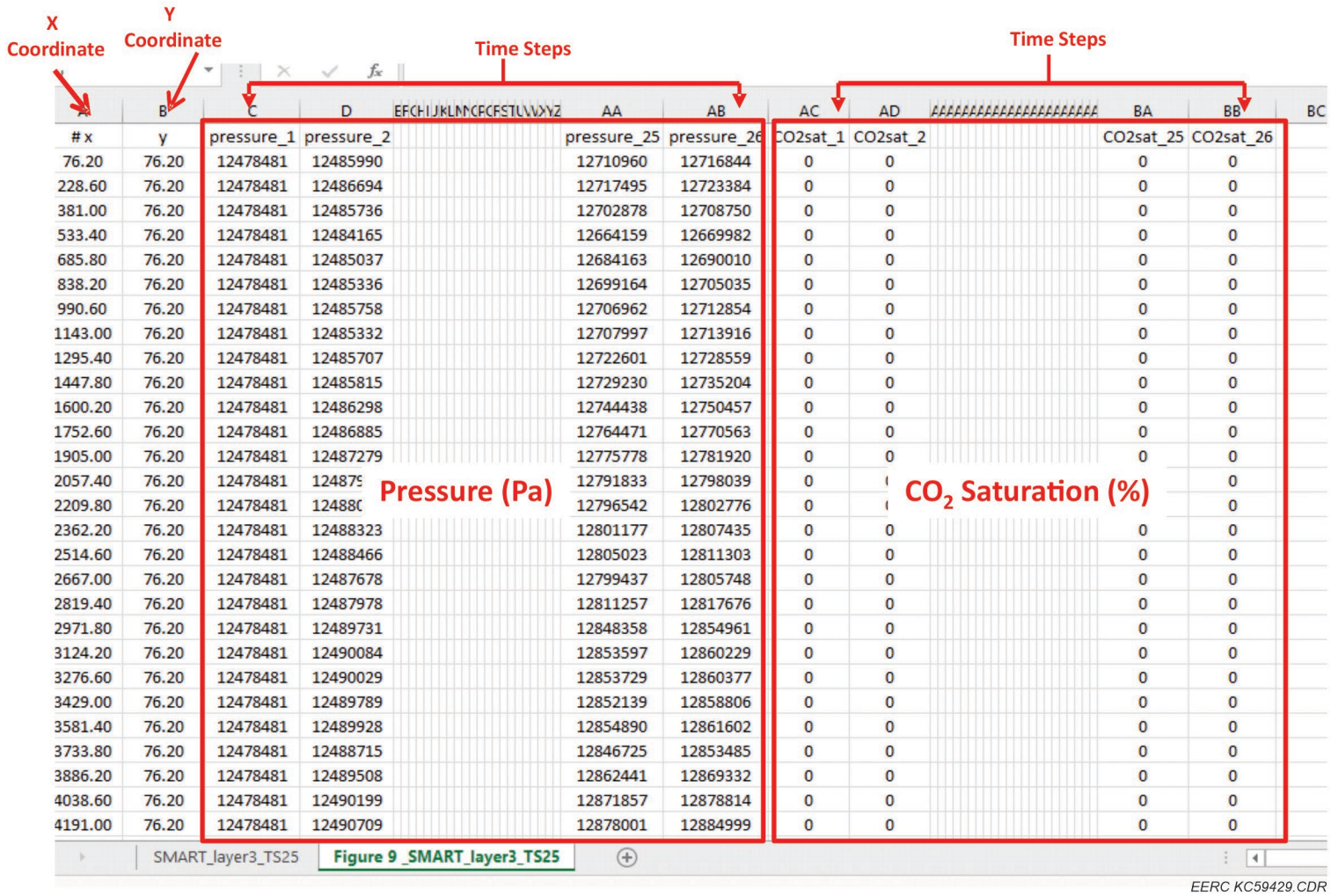

# x	y	pressure_1	pressure_2	pressure_25	pressure_26	CO2sat_1	CO2sat_2	CO2sat_25	CO2sat_26
76.20	76.20	12478481	12485990	12710960	12716844	0	0	0	0
228.60	76.20	12478481	12486694	12717495	12723384	0	0	0	0
381.00	76.20	12478481	12485736	12702878	12708750	0	0	0	0
533.40	76.20	12478481	12484165	12664159	12669982	0	0	0	0
685.80	76.20	12478481	12485037	12684163	12690010	0	0	0	0
838.20	76.20	12478481	12485336	12699164	12705035	0	0	0	0
990.60	76.20	12478481	12485758	12706962	12712854	0	0	0	0
1143.00	76.20	12478481	12485332	12707997	12713916	0	0	0	0
1295.40	76.20	12478481	12485707	12722601	12728559	0	0	0	0
1447.80	76.20	12478481	12485815	12729230	12735204	0	0	0	0
1600.20	76.20	12478481	12486298	12744438	12750457	0	0	0	0
1752.60	76.20	12478481	12486885	12764471	12770563	0	0	0	0
1905.00	76.20	12478481	12487279	12775778	12781920	0	0	0	0
2057.40	76.20	12478481	12487	12791833	12798039	0			0
2209.80	76.20	12478481	12488	12796542	12802776	0			0
2362.20	76.20	12478481	12488323	12801177	12807435	0	0	0	0
2514.60	76.20	12478481	12488466	12805023	12811303	0	0	0	0
2667.00	76.20	12478481	12487678	12799437	12805748	0	0	0	0
2819.40	76.20	12478481	12487978	12811257	12817676	0	0	0	0
2971.80	76.20	12478481	12489731	12848358	12854961	0	0	0	0
3124.20	76.20	12478481	12490084	12853597	12860229	0	0	0	0
3276.60	76.20	12478481	12490029	12853729	12860377	0	0	0	0
3429.00	76.20	12478481	12489789	12852139	12858806	0	0	0	0
3581.40	76.20	12478481	12489928	12854890	12861602	0	0	0	0
3733.80	76.20	12478481	12488715	12846725	12853485	0	0	0	0
3886.20	76.20	12478481	12489508	12862441	12869332	0	0	0	0
4038.60	76.20	12478481	12490199	12871857	12878814	0	0	0	0
4191.00	76.20	12478481	12490709	12878001	12884999	0	0	0	0

Figure 9. LUT_RROMGen_reservoirdata.csv file containing *x*- and *y*-coordinates of the 211 × 211 grid cells in the first two columns and subsequent columns with pressure and CO_2 saturation data for each time step varying over 25-year period, including 0-time step at the beginning.

The LUT Reservoir Component requires three additional inputs to describe the petrophysical properties of the storage reservoir and shale units (Table 1):

- Parameter 1 (logResPerm): logarithm of the storage reservoir permeability in m^2
- Parameter 2 (reservoirPorosity): porosity of the storage reservoir expressed as a fraction
- Parameter 3 (logShalePerm): logarithm of the shale unit permeability in m^2

The storage reservoir and shale permeability were estimated by taking the geometric mean of the CMG GEM model layer, resulting in logResPerm and logShalePerm values of −13.6 and −18.0 m^2 (24.64 and 0.001 mD), respectively. The reservoirPorosity was estimated by taking the arithmetic average of the CMG GEM model layer, resulting in 0.149 (Table 1). The LUT Reservoir Component allows the user to specify either a fixed value or a statistical distribution for logResPerm, reservoirPorosity, and logShalePerm. Fixed values of logResPerm, reservoirPorosity, and logShalePerm were used for all Open-IAM testing.

Table 1. LUT Reservoir Component Petrophysical Parameters Used in the Open-IAM Testing

Petrophysical Parameter	Value
logResPerm [log(m^2)]	−13.6
reservoirPorosity (fraction)	0.149
logShalePerm [log(m^2)]	−18.0

The last step for the LUT Reservoir Component is to select the outputs, which in this case were Pressure [Pa] and CO_2 saturation [-]. The simulation result of the LUT Reservoir Component produces output pressure and CO_2 saturation values at the top of the storage reservoir at each wellbore location. These LUT Reservoir Component outputs are then used as inputs to the MSW Component to simulate vertical leakage through one or more wellbores.

Multisegmented Wellbore Component

The (MSW) Component allows the Open-IAM to assign multiple hypothetical leaky wells as potential vertical leakage pathways that connect the storage reservoir to the overlying aquifer systems. The MSW Component estimates the leakage rates (kg/s) of CO_2 and brine from the storage reservoir to the overlying aquifer units. It integrates output files from the LUT Reservoir Component and simulates fluid flow across the formation units using the solutions of Celia and others (2011). The underlying equations in the MSW Component assume that vertical leakage occurs via the annulus between the outside of the casing and borehole because of potential cracks and/or corrosion in the cement within the casing–formation interface. The solution does not consider discrete features or other vertical flow paths such as fractures or cracks in the formation units. The model uses a one-dimensional multiphase version of Darcy's law to represent flow along a leaky well (Celia and others, 2011).

The MSW Component includes nine parameter inputs to define the solution for vertical wellbore leakage (Figure 10). The user may enter each parameter as either a fixed value or a statistical distribution. For the Open-IAM testing, aquifer permeability (referring to the Aquifer 1 [Thief zone] and Aquifer 2 [USDW] permeability, not the permeability of the storage reservoir), leaky wellbore radius, the brine density and viscosity, CO_2 density and viscosity, and brine saturation and compressibility were entered as fixed values representing average pressure, temperature, and/or salinity conditions. However, leaky wellbore effective permeability was treated as a probabilistic input using a triangular distribution. The triangular distribution is a continuous probability distribution with Lower Limit a, Upper Limit b, and Mode c (most likely estimate), where $a < b$ and $a \leq c \leq b$. The triangular distribution is commonly used in risk assessment when not much is known about the distribution of an outcome besides its smallest and largest values and the most likely outcome (Fenton and Neil, 2013).

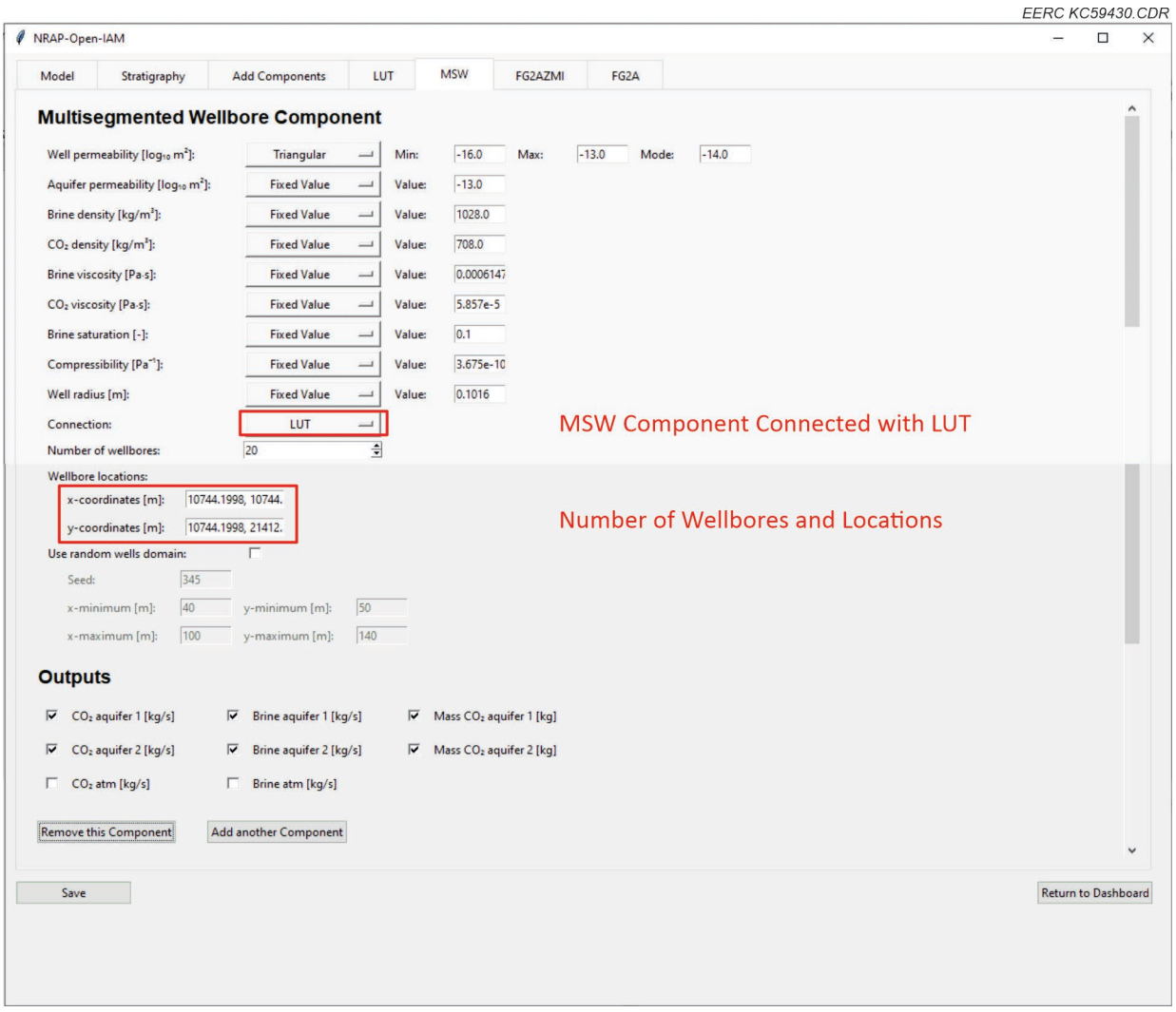

Figure 10. Input parameters for the MSW Component.

Table 2 summarizes the input parameters and values for the MSW Component used in the Open-IAM testing. Carey (2017) provides probability distributions for the effective permeability of potentially leaking wells at storage sites, estimating a wide range from 10^{-10} to 10^{-20} m^2. The values used in the Open-IAM testing of 10^{-13} to 10^{-16} m^2 (with a mode of 10^{-14} m^2) reflect a conservative range with greater effective permeability than used in the Alberta, FutureGen, and Gulf of Mexico models described by Carey (2017). In other words, the effective permeability values used in the Open-IAM testing were selected to provide an upper-bound estimate of potential leakage of CO_2 and brine that would result in outputs for visualization; real-world applications representing actual storage projects may elect to use lower effective permeability values.

The MSW Component provides the user with a dropdown menu ("Connection") to select the inputs of pressure (Pa) and CO_2 saturation data (%) either from the LUT Reservoir Component or from dynamic parameters (Figure 10 – "MSW Component connected with LUT"). Dynamic parameters are only applicable if the MSW Component is specified without connecting the LUT Reservoir Component and were, therefore, not considered for the Open-IAM testing.

Table 2. List of MSW Component Parameters Used in the Open-IAM Testing

Input Parameters	Min	Max	Mode or Fixed Value	Distribution Type
Well Permeability [$\log_{10}m^2$]	−16	−13	−14	Triangular
Aquifer Permeability [$\log_{10}m^2$]			−13	Fixed value
Brine Density [kg/m^3]			1028	Fixed value
CO_2 Density [kg/m^3]			708	Fixed value
Brine Viscosity [Pa-s]			6.147E-04	Fixed value
CO_2 Viscosity [Pa-s]			5.857E-05	Fixed value
Brine Saturation [-]			0.1	Fixed value
Compressibility [Pa^{-1}]			3.675E-10	Fixed value
Well Radius [m]			0.1016	Fixed value

For heuristic, what-if scenario modeling, 20 hypothetical leaky wells placed within the study area were used to simulate the leakage scenarios using the MSW Component. Four of these leaky wells (LW-1 to LW-4) were colocated with the four injection wells (IW-1 to IW-4) (Figure 11). In the MSW Component, the *x*- and *y*-coordinates of each well were entered into their respective fields as a string separated by commas (Figure 10).

The last step for the MSW Component is to select the Outputs. The Outputs selected for testing were leakage rates (kg/s) of CO_2 and brine and leaked mass (kg) of CO_2 to Aquifer 1 (Thief zone) and Aquifer 2 (USDW) (Figure 10). Once the LUT Reservoir Component and MSW Component are defined, the next step is to define the aquifer components of the model.

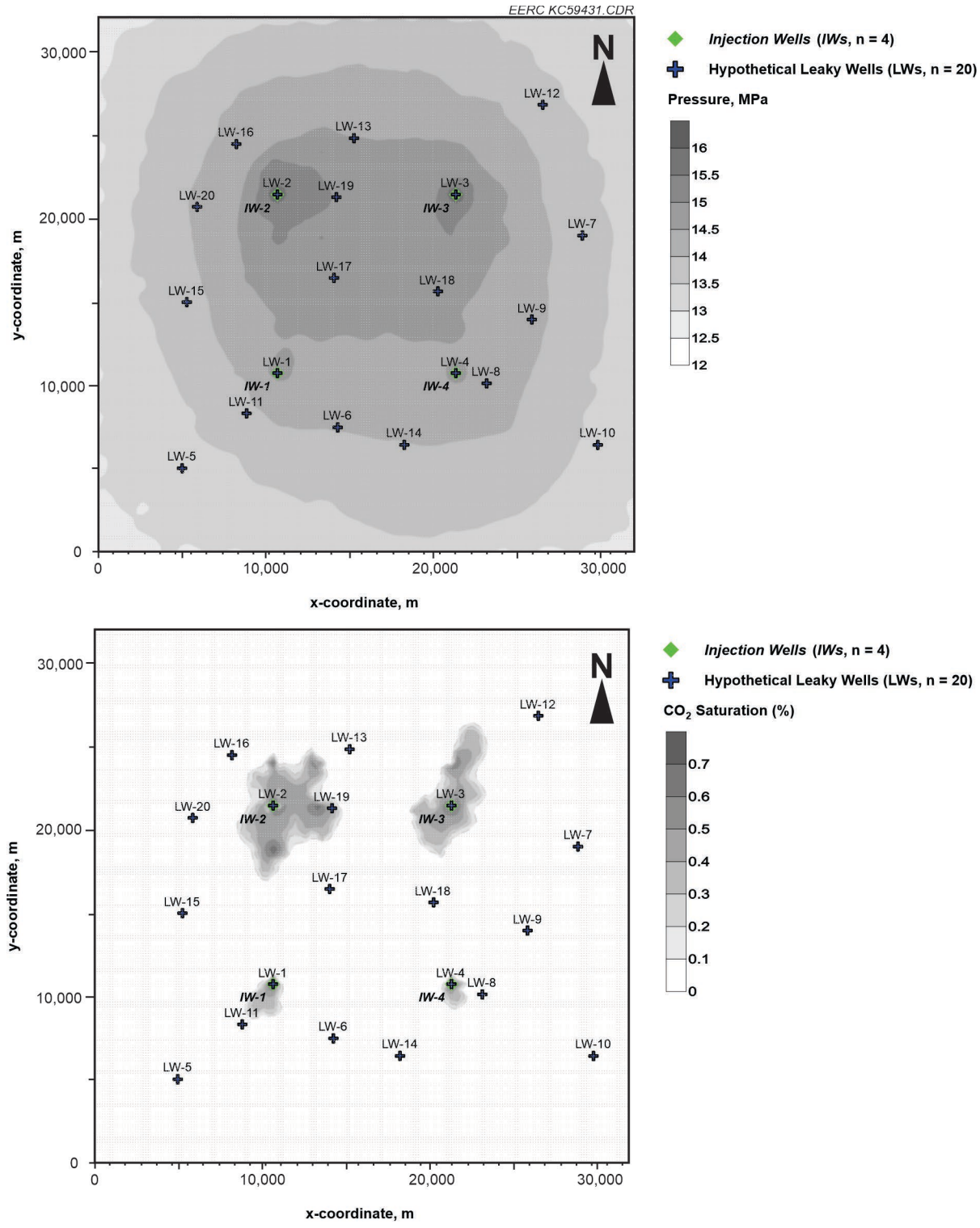

Figure 11. Maps showing the Open-IAM study site (211 × 211 grid cells) with pressure (a – top panel) and CO_2 saturation (b – bottom panel) at the end of the 25-year CO_2 injection period and the locations of four injection wells (IW-1 to IW-4) and twenty hypothetical leaky wells (LW-1 to LW-20) used in the Open-IAM testing.

FutureGen 2.0 AZMI Component

The FutureGen 2.0 AZMI Component is based on a nonisothermal aquifer simulation conducted as a part of monitoring program that was designed, developed, and implemented at the FutureGen 2.0 site (Vermeul et al., 2016) to track and account for the mass of CO_2 injected and to protect USDWs from storage-related impacts. The FutureGen 2.0 AZMI Component is a regression model fitted to the results of STOMP-CO2E-R multiphase flow and reactive transport simulations of CO_2 and brine leakage (Vasylkivska et al., 2021). The AZMI regression model training simulations were performed for aquifers with depths ranging from 700 to 1600 m and an aquifer thickness ranging from 30 to 90 m. Therefore, the FutureGen 2.0 AZMI Component was used for modeling Aquifer 1 (Thief zone with a depth of 942 m and a thickness of 54 m). The term "above-zone monitoring interval (AZMI)" is synonymous with "thief zone" used in the current document.

The FutureGen 2.0 AZMI Component predicts the size of "impact plumes" according to five metrics: pH, total dissolved solids (TDS), pressure, dissolved CO_2, and temperature and defines the volume (m^3) and dimensions (m) in the *x*- (length), *y*- (width), and *z*-direction (height) (dx/dy/dz) of the impact plumes.

The FutureGen 2.0 AZMI Component requires four input parameters: aquifer porosity, aquifer horizontal permeability, anisotropy ratio, and the volume fraction of calcite (Figure 12). The user may enter each parameter as either a fixed value or a statistical distribution. For the Open-IAM testing, the aquifer porosity, horizontal permeability ($\log_{10}[m^2]$), anisotropy ratio ($\log_{10}$), and volume fraction of calcite were entered as fixed values representing average values of the aquifer porosity, permeability, and unique geochemical/mineralogical composition (Table 3).

The FutureGen 2.0 AZMI Component provides the user with a dropdown menu to connect the MSW Component (defined in the Multisegmented Wellbore Component section) and to select "Aquifer 1" as defined in the Stratigraphy Component (defined in the Stratigraphy Component section).

The Outputs selected for testing were volume (m^3) and dimensions (m; length [dx], width [dy], and height [dz]) of impact plumes of pH, TDS, pressure, and dissolved CO_2 (Figure 12). Temperature was not selected as an output for testing to limit the number of outputs and reduce postprocessing time.

Table 3. List of FutureGen 2 AZMI/FutureGen 2 Aquifer Component Parameters Used in the Open-IAM Testing

Input Parameters	Value	Distribution Type
Aquifer Porosity [-]	0.2	Fixed value
Horizontal Permeability [$\log_{10} m^2$]	−12.6	Fixed value
Anisotropy Ratio [$\log_{10}$]	0.5	Fixed value
Volume Fraction of Calcite [-]	0.0	Fixed value

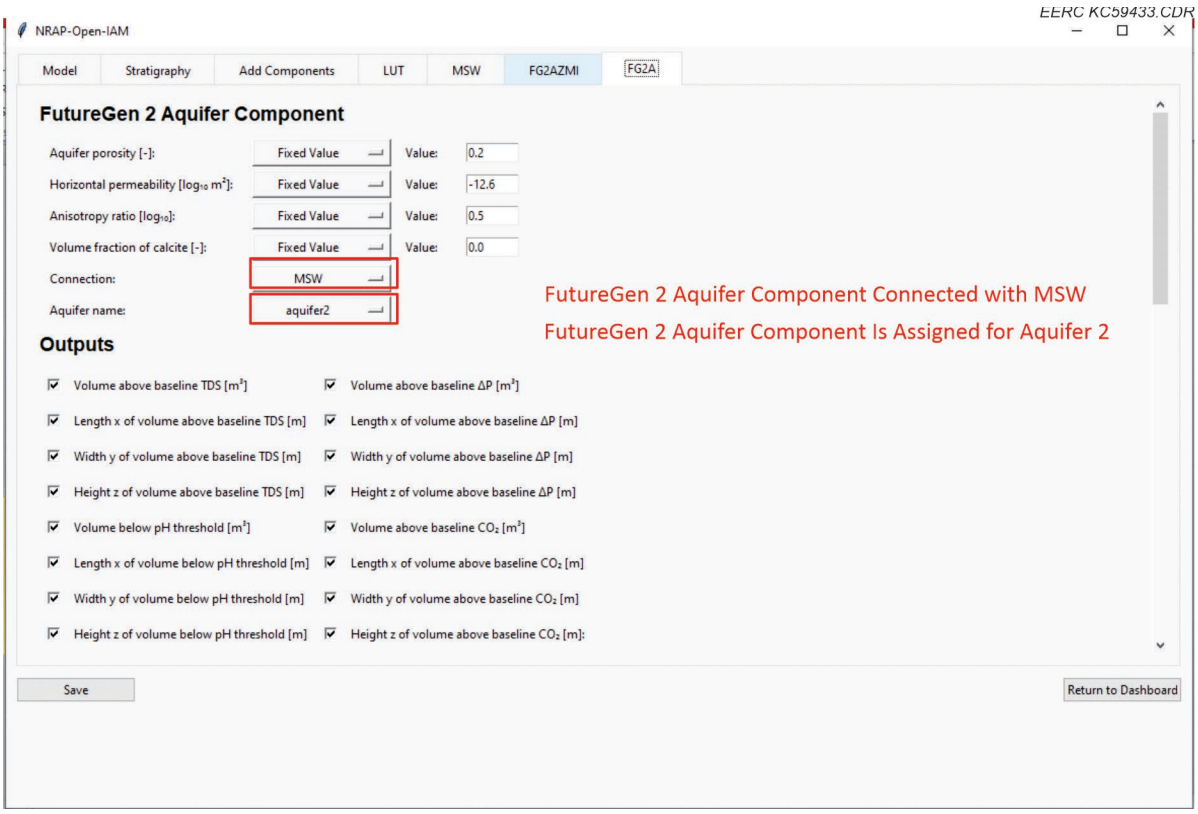

Figure 12. Input parameter for the FutureGen 2.0 AZMI Component.

FutureGen 2.0 Aquifer Component

The FutureGen 2.0 Aquifer Component is also a regression model fitted to the results of STOMP-CO2E-R multiphase flow and reactive transport simulations of CO_2 and brine leakage (Vasylkivska et al., 2021). The FutureGen 2.0 Aquifer Component is like the FutureGen 2.0AZMI Component but is focused on four metrics: pH, TDS, pressure, and dissolved CO_2. The FutureGen 2.0 Aquifer Component does not include temperature as a metric. In addition, the FutureGen 2.0 Aquifer Component is recommended for aquifer depths from 100 to 700 m, which is shallower than the FutureGen 2.0 AZMI Component (700 to 1600 m). Therefore, the FutureGen 2.0 Aquifer Component was used for modeling Aquifer 2 (USDW with a depth of 237 m and a thickness of 65 m).

Identical to the FutureGen 2.0 AZMI Component, the FutureGen 2.0 Aquifer Component includes four parameter inputs to define the aquifer properties and mineralogical composition: aquifer porosity, aquifer horizontal permeability, anisotropy ratio, and the volume fraction of calcite (Figure 13, Table 3). For the Open-IAM testing, the aquifer porosity, horizontal permeability ($\log_{10}[m^2]$), anisotropy ratio ($\log_{10}$), and volume fraction of calcite were entered as fixed values representing average values of the aquifer porosity, permeability, and unique geochemical/mineralogical composition (Table 3).

The FutureGen 2.0 Aquifer Component also provides the user a dropdown menu to connect MSW Component (defined in the Multisegmented Wellbore Component section) and to select "Aquifer 2" as defined in the Stratigraphy Component (defined in the Stratigraphy Component section).

The Outputs selected for testing were volume (m^3) and dimensions (m; length [dx], width [dy], and height [dz]) of impact plumes of pH, TDS, pressure, and dissolved CO_2 (Figure 13).

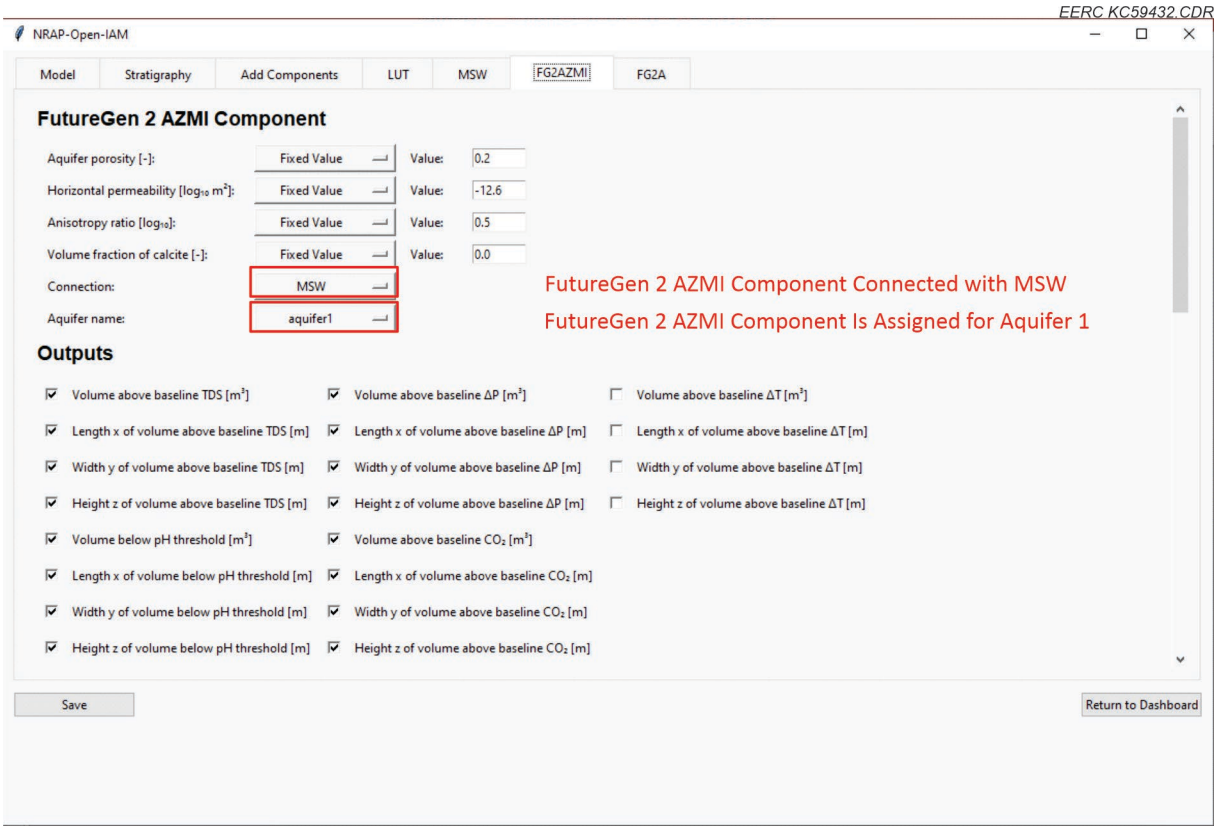

Figure 13. Input parameter for the FutureGen 2 Aquifer Component.

Once the FutureGen 2.0 AZMI Component and FutureGen 2.0 Aquifer Component are defined and connected to the MSW Component, the next steps are to save the model and return to the Open-IAM Main Page, run the Open-IAM simulation, and conduct postprocessing of the results. At this point, the Open-IAM model now contains a Stratigraphy Component, LUT Reservoir Component, MSW Component, and two Aquifer Components, which form the storage complex for the Open-IAM simulations.

Run Simulation and Postprocessing

The saved model was executed from the Open-IAM Main Page using the tab "RUN SIMULATION" button (Figure 14). After running the simulation, the Open-IAM stores all the simulated results as text files, including pressure and CO_2 saturation from the LUT Reservoir Component, CO_2 and brine leakage rates to Aquifer 1 and Aquifer 2 from the MSW Component, and volume and dimensions of impact plumes to Aquifer 1 and Aquifer 2 from the FutureGen 2.0 AZMI and Aquifer Components, respectively, for each of the 20 leaky wellbores. The output text files are named *LHS_results.txt* and *LHS_statistics.txt* and are saved in the Open-IAM simulation output directory. The *LHS_results.txt* file includes the time-series results for each individual realization. For example, if the user specified a size of 100 in the Model Component for the LHS analysis, then the *LHS_results.txt* would include CO_2 and brine leakage results of each realization for each of the 20 leaky wellbores for Aquifer 1 and Aquifer 2 and each time step (i.e., 100 outputs for each time step, leaky wellbore, and aquifer combination). The *LHS_statistics.txt* file includes descriptive statistics across all realizations from the LHS analysis. These descriptive statistics include the minimum (min), maximum (max), arithmetic average (mean), standard deviation (stdev), and variance, in addition to five quantile estimates: 2.5th, 5th, 50th, 95th, and 97.5th percentiles.

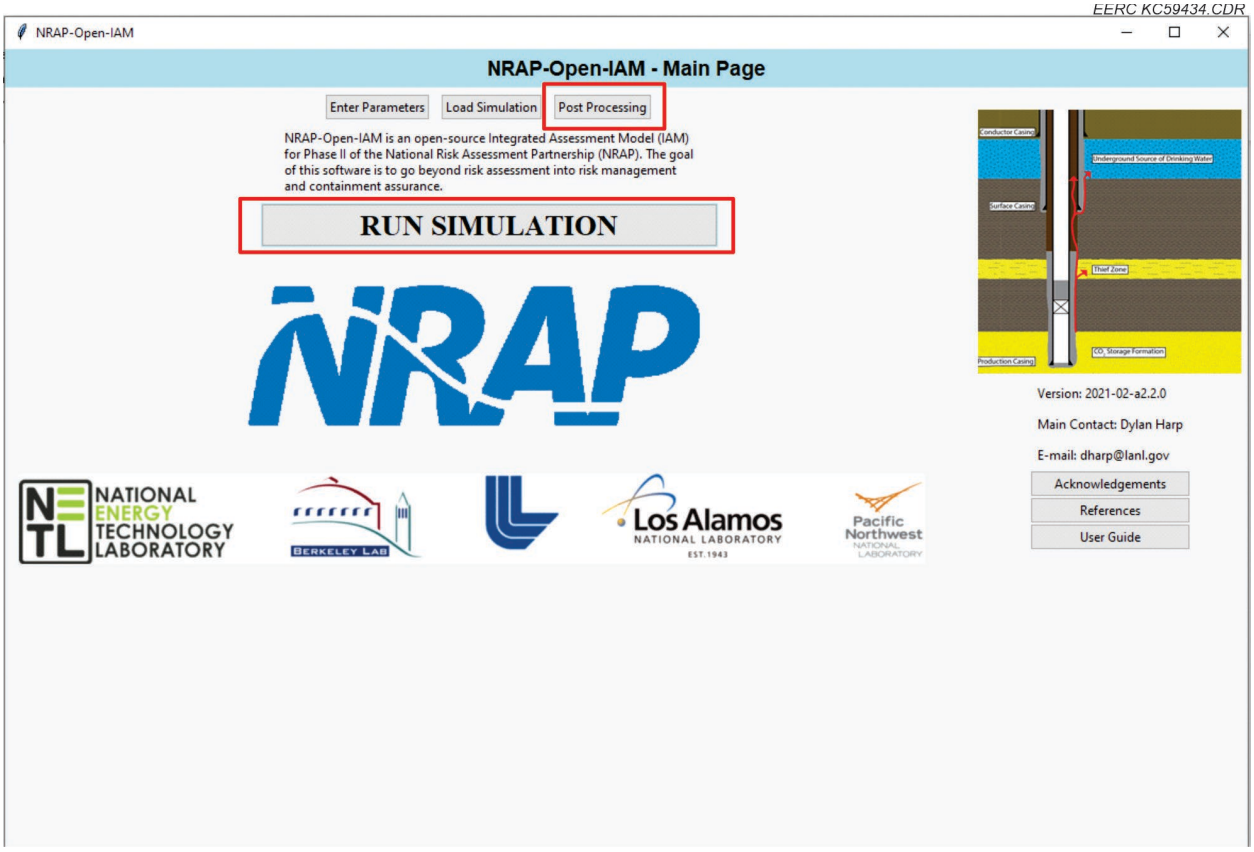

Figure 14. Open-IAM Main Page showing the buttons used to Run Simulation and conduct Post Processing of the results to complete the Open-IAM testing simulation.

The user may explore the output files using built-in postprocessing functions within Open-IAM or analyze the *LHS_results.txt* and *LHS_statistics.txt* files using software programs outside of Open-IAM. The button "Post Processing" in the Open-IAM Main Page can generate plots of the results as .png files and save these files in the same Open-IAM simulation output directory. At the time of this report, the built-in postprocessing functions within Open-IAM were relatively limited; therefore, the results were exported from Open-IAM into Microsoft Excel or Minitab (Minitab 19 Statistical Software, 2020) for visualization and analysis.

OPEN-IAM SIMULATION RESULTS

This section describes the outputs from a complete example of an Open-IAM simulation based on the preceding discussion of inputs, which are summarized below:

- 25-year CO_2 injection period-in-time steps of 1 year.
- LHS analysis of size = 100 realizations.
- Generalized storage complex stratigraphy based on work conducted under Task 4 of the SMART-CS Initiative, which includes a storage reservoir, primary seal (cap rock) (Shale 1), intermediate saline aquifer or thief zone (Aquifer 1), secondary seal (Shale 2), USDW (Aquifer 2), and final shale unit (Shale 3) (Figure 4).
- LUT Reservoir Component based on the pressure and CO_2 saturation results of a numerical reservoir simulation conducted in CMG GEM, processed through Petrel, and postprocessed in Python to create the input .csv files for Open-IAM (Figure 9).
- MSW Component with 20 hypothetical leaky wellbores located within the study area; leaky wellbore radius, aquifer permeability (referring to the Aquifer 1 and Aquifer 2 permeability, not the permeability of the storage reservoir), the brine density and viscosity, CO_2 density and viscosity, and brine saturation and compressibility entered as fixed values; and only the leaky wellbore permeability was treated as a probabilistic input using a triangular distribution.
- FutureGen 2.0 AZMI Component used for Aquifer 1 because of its depth ($700 \leq 942–996 \leq 1600$ m) and FutureGen 2.0 Aquifer Component for Aquifer 2 because of its depth ($100 \leq 238–302 \leq 700$ m). All the input parameters (aquifer porosity, horizontal permeability, anisotropic ratio, volume fraction of calcite) are the same for both FutureGen 2.0 components and entered as fixed values.

Figure 15 illustrates the workflow and components for the Open-IAM simulations using these inputs. The first three boxes at the top were used to 1) create physics-based reservoir simulations of pressure and CO_2 saturation using CMG GEM, 2) export the simulation results from CMG GEM to Petrel for conversion into a Gslib-formatted output file in ASCII, and 3) run the ASCII file through a Python script to create an Open-IAM input .csv file. These three steps were

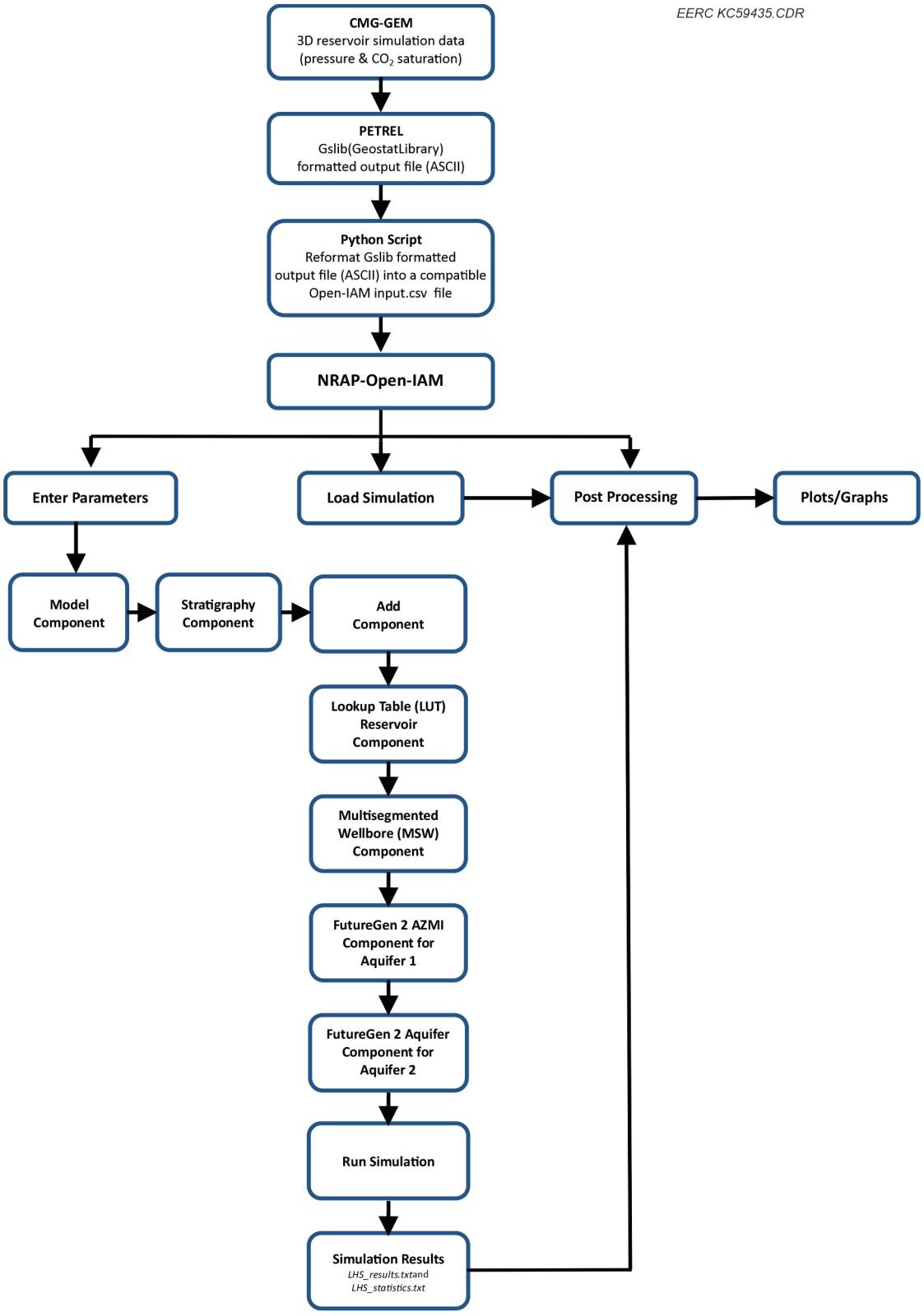

Figure 15. Workflow diagram showing the components used in the Open-IAM testing.

conducted outside of Open-IAM but would be required for any new project relying on numerical reservoir simulation to generate the input data. Next, since the testing involved building a new Open-IAM model, the workflow went to the left – Enter Parameters – and proceeded to complete the Model Component and Stratigraphy Component, and then to add the remaining components: Lookup Table Reservoir Component (using the CMG GEM results and converted input .csv files to represent the time-series pressure and CO_2 saturation in the reservoir), Multisegmented Wellbore Component (to create hypothetic leaky wellbores in the system that penetrate the full storage complex stratigraphy), FutureGen 2.0 AZMI Component (to model impacts to the Aquifer 1 thief zone), and FutureGen 2.0 Aquifer Component (to model impacts to the Aquifer 2 USDW). Lastly, the Open-IAM model was saved, and Run Simulation was executed to generate Open-IAM simulation results (LHS_results.txt and LHS_statistics.txt output files). The Open-IAM simulation results could be examined within Open-IAM using the Post Processing feature; however, in this testing, the output files were investigating outside of Open-IAM using Excel and Minitab to create plots and graphs. If the user was not creating a new Open-IAM model but instead wanted to load a previous simulation, then the user could simply use the Load Simulation feature and then proceed to the Post Processing step.

Comparing CMG GEM and Open-IAM

The 20 hypothetical leaky wellbores, LW-1 through LW-20, were randomly distributed across the study area at varying distances from the four CO_2 injection wells. LW-1 through LW-4 were colocated with the injection wells, IW-1 to IW-4, and, therefore, were expected to represent the worst-case wellbore leakage scenarios where CO_2 and/or brine migrate vertically through the annulus of the injectors. While LW-1, LW-2, LW-3, LW-4, and LW-19 were located within the areal extent of the CO_2 plume area by the end of 25 years, the other leaky wells (LW-5 to LW-18 and LW-20) were located beyond the CO_2 plume at different distances (Figure 11). The first evaluation of the Open-IAM outputs was to compare the Open-IAM simulated reservoir pressure and CO_2 saturation at each wellbore *x*- and *y*-coordinate to the CMG GEM data (processed through Petrel and Python script) to ensure the accuracy of the LUT Reservoir Component interpolations. As shown below, the Open-IAM simulations of reservoir pressure (Figure 16a) and CO_2 saturation (Figure 16b) for the four hypothetical leaky well locations: LW-1, LW-2, LW-3, and LW-4 over 25 years matched the CMG GEM input data; i.e., the lines from the Open-IAM output overlay the plus symbols from CMG GEM output.

As would be expected, the CO_2 saturations in the storage reservoir were zero for the wells located beyond the CO_2 plume (LW-5 to LW-18 and LW-20; Figure 17), while the time-series progression of CO_2 saturation in the storage reservoir at the LW-1, LW-2, LW-3, LW-4, and LW-19 locations were consistent with their spatial relationship to the CO_2 plume; i.e., CO_2 arrived instantaneously at LW-1, LW-2, LW-3, and LW-4 in Year 1 and then arrived much later at LW-19 in Year 21 (Figure 17).

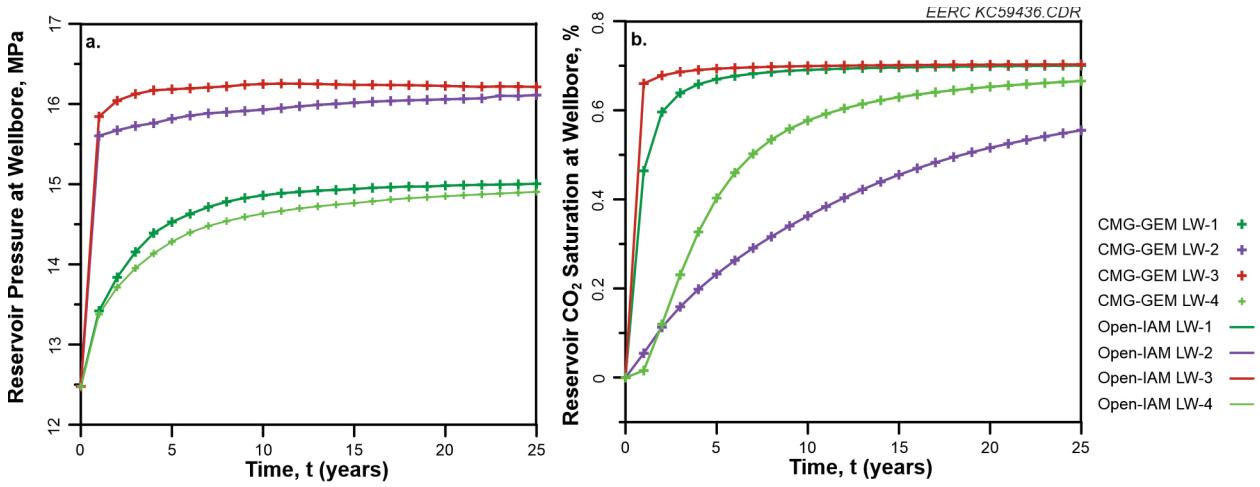

Figure 16. Storage reservoir pressure (a – left panel) and CO_2 saturation (b – right panel) with time at the four hypothetical leaky wells showing comparisons between the CMG GEM outputs (processed through Petrel and Python script) and the Open-IAM simulations.

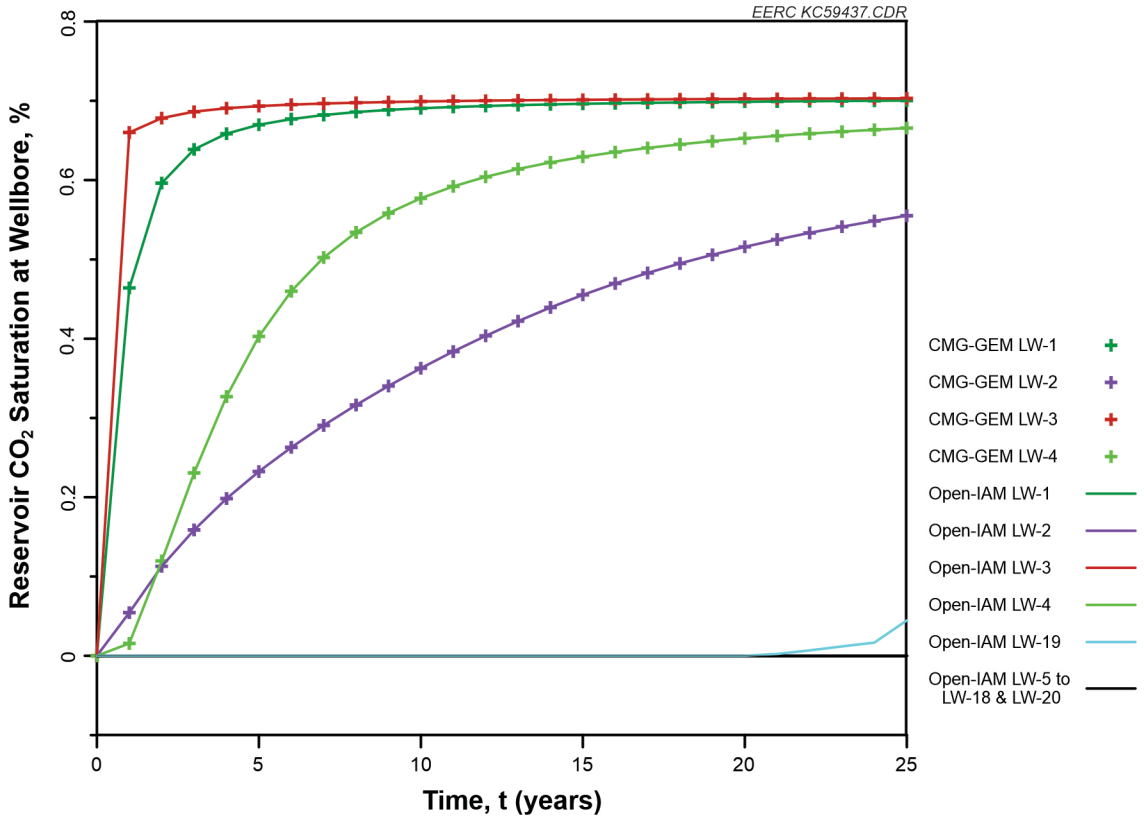

Figure 17. Storage reservoir CO_2 saturation with time at the twenty hypothetical leaky wells showing CO_2 saturations in the storage reservoir were zero for the wells located beyond the CO_2 plume (LW-5 to LW-18, LW-20). The CO_2 arrived at LW-1, LW-2, LW-3, and LW-4 instantaneously in Year 1 but did not reach LW-19 until Year 21.

Evaluating Time-Series Leakage Rates to Aquifers 1 and 2

CO_2 Leakage Rates at LW-1, LW-2, LW-3, LW-4, and LW-19

Figure 18 shows the time-series CO_2 leakage rates from the storage reservoir into Aquifer 1 (Thief zone) and Aquifer 2 (USDW) at LW-1, LW-2, LW-3, LW-4, and LW-19 (the five of the 20 hypothetical leaky wellbores that were located within the CO_2 plume during the 25-year injection period). The CO_2 leakage rate at all other wells was zero since these wells were located beyond the CO_2 plume. The user-defined uncertainty in the leaky well permeability resulted in variation across realizations, as shown by the gray lines for each of the 100 realizations. The red lines in all the panels show a LOWESS (locally weighted scatterplot smoothing) smoother using a span width of 10% to illustrate a most likely result for each time step (1-year increments from Years 1 to 25). The *y*-axes are shown on a $\log_{10}$-scale to permit comparative assessments between Aquifer 1 and Aquifer 2, since the leakage rates between these groups varied by log-orders.

LW-2 was colocated with the injection well, IW-2, which had the largest CO_2 plume, making it a relatively worst-case scenario for potential CO_2 leakage in terms of proximity to CO_2 saturation in the storage reservoir. LW-2 had the highest CO_2 leakage rates to Aquifer 1 and Aquifer 2 of −3.5 and −3.9, respectively, on a $\log_{10}$-scale (0.000349 and 0.000113 kg/s, respectively). The median CO_2 leakage rates were more than an order-of-magnitude lower than the maximum, and were −4.7 and −5.2, respectively, on a $\log_{10}$-scale (0.000020 and 0.000006 kg/s, respectively). Therefore, the user-defined uncertainty in the leaky well permeability – three orders-of-magnitude from 10^{-13} to 10^{-16} m^2 (with a mode of 10^{-14} m^2) – resulted in approximately 1.2 to 1.3 log-orders of variation between the median and maximum CO_2 leakage rates at LW-2 (Figure 18).

LW-1, LW-3, and LW4 were collocated with injection wells IW-1, IW-3, IW-4, respectively, and therefore also represent relatively worst-case scenarios for potential CO_2 leakage in terms of proximity to CO_2 saturation in the storage reservoir. The maximum simulated CO_2 leakage rates to Aquifer 1 were −3.6, −3.5, and −3.6, respectively, on a $\log_{10}$-scale (0.000232, 0.000323, and 0.000225 kg/s, respectively. The median CO_2 leakage rates were −4.8, −4.6 and −4.8, respectively, on a $\log_{10}$-scale (0.000017, 0.000025, and 0.000015 kg/s, respectively). The CO_2 leakage rates to Aquifer 2 were −4.0, −4.1, and −4.0 respectively, on a $\log_{10}$-scale (0.000091, 0.000084, and 0.000095 kg/s, respectively), more than an order-of-magnitude lower than the maximum observed in the Aquifer 1 (Figure 18). The maximum CO_2 leakage rates to Aquifer 1 across LW-1, LW-2, LW-3, and LW-4 (−3.6, −3.5, −3.5, and −3.6, respectively, on a $\log_{10}$-scale) were essentially equivalent, and the maximum CO_2 leakage rates to Aquifer 2 across LW-1, LW-2, LW-3, and LW-4 (−4.0, −3.9, −4.1, and −4.0, respectively, on a $\log_{10}$-scale) were also essentially equivalent.

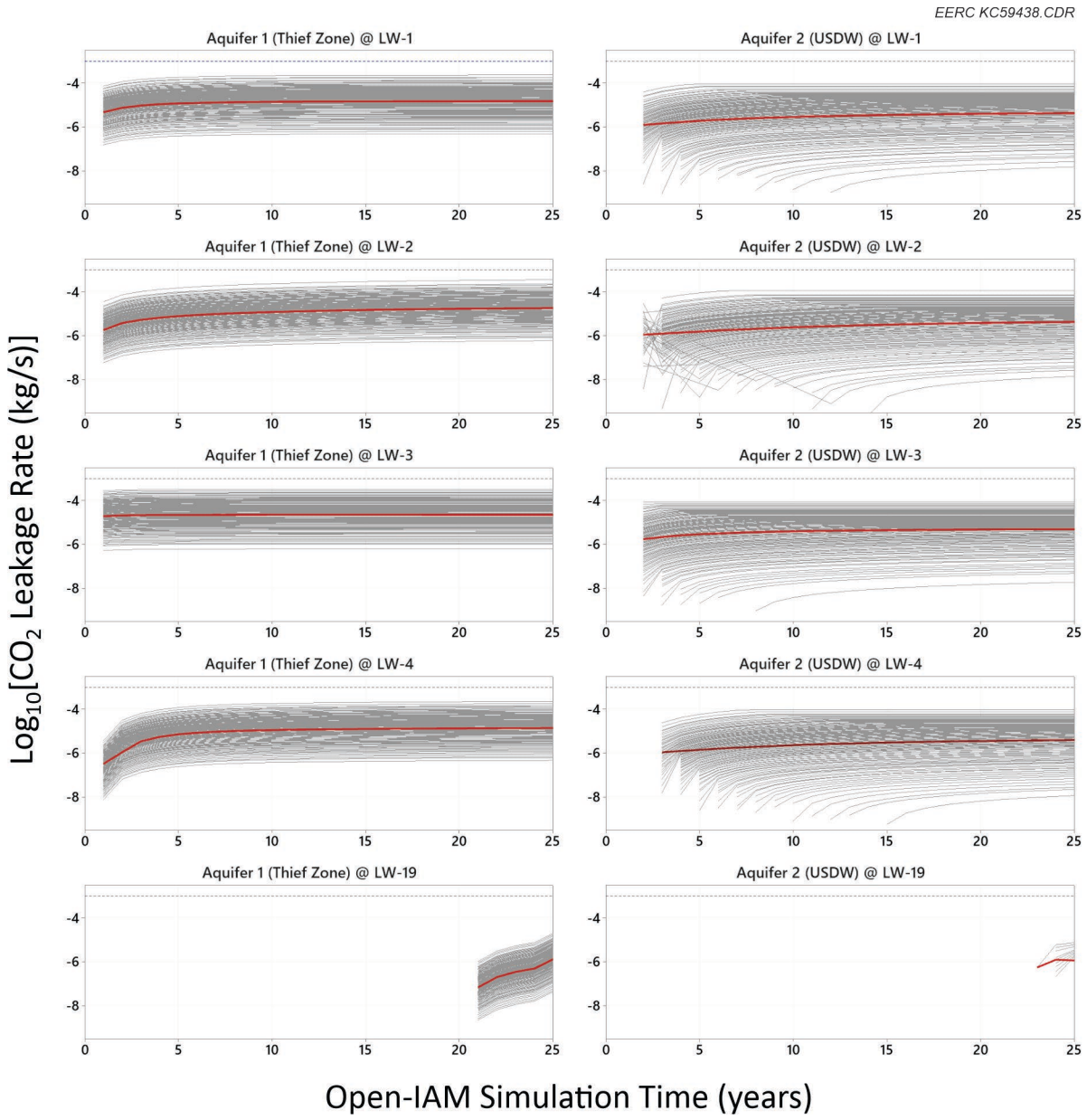

Figure 18. Open-IAM simulated CO_2 leakage rates from the storage reservoir into Aquifer 1 (Thief zone – left column) and Aquifer 2 (USDW – right column) at LW-1, LW-2, LW-3, LW-4, and LW-19. The gray lines show each of the 100 realizations, and the red lines show a LOWESS smoother using a span width of 10%. Blue reference horizontal lines at y = −3 (0.001 kg/s) have been added to each panel to aid visualization (note: the *y*-axis is on a $\log_{10}$-scale and, therefore, zero values are not plotted).

LW-19 was located near the perimeter of the CO_2 plume extent surrounding IW-2, approximately 2.5 miles east of Injection Well IW-2. Consequently, arrival of the CO_2 plume in the storage reservoir at LW-19 did not occur until approximately 21 years into the injection operation; therefore, arrival of CO_2 leakage into Aquifer 1 and Aquifer 2 at LW-19 did not occur until approximately 21 and 23 years, respectively, during the injection operation (Figure 18). After 21 years of injection operation, the maximum simulated CO_2 leakage rates to Aquifer 1 and Aquifer 2 at LW-19 were −4.7 and −5.1, respectively, on a $\log_{10}$-scale (0.000020 and 0.000007 kg/s, respectively). The median CO_2 leakage rates were approximately an order-of-magnitude lower than the maximum and were −5.8 and −5.7, respectively, on a $\log_{10}$-scale (0.000001 and 0.000002 kg/s, respectively).

Brine Leakage Rates at LW-1, LW-2, LW-3, LW-4, and LW-19

Figure 19 uses the same formatting conventions as Figure 18 and shows the time-series brine leakage rates from the storage reservoir into Aquifer 1 (Thief zone) and Aquifer 2 (USDW) at the same set of leaky wellbores: LW-1, LW-2, LW-3, LW-4, and LW-19.

At LW-2, the maximum simulated brine leakage rates to Aquifer 1 and Aquifer 2 were −4.2 and −6.5, respectively, on a $\log_{10}$-scale (0.000068 and 0.0000003 kg/s, respectively). The median brine leakage rates were more than an order-of-magnitude lower than the maximum and were −5.4 and less than −7.9, respectively, on a $\log_{10}$-scale (0.000004 and <0.00000001 kg/s, respectively). Therefore, like the results for the CO_2 leakage rates, the user-defined uncertainty in the leaky well permeability – three orders-of-magnitude from 10^{-13} to 10^{-16} m^2 (with a mode of 10^{-14} m^2) – resulted in approximately 1.2 to 1.4 log-orders of variation between the median and maximum brine leakage rates at LW-2 (Figure 19).

At LW-1, LW-3, and LW4, the maximum simulated brine leakage rates to Aquifer 1 were −5.1, −4.9 and −4.7, respectively, on a $\log_{10}$-scale (0.000007, 0.000012, and 0.000020 kg/s, respectively). The median brine leakage rates were −6.3, −6.0, and −5.9, respectively, on a $\log_{10}$-scale (0.0000005, 0.0000009, and 0.0000014 kg/s, respectively). The maximum brine leakage rates to Aquifer 2 were lower than that of Aquifer 1 and were −6.6, −7.0 and −6.6 respectively, on a $\log_{10}$-scale (0.0000002, 0.0000001, and 0.0000003 respectively), lower than the maximum observed in the respective leaky wells. The median brine leakage rates were less than −7.8 on a $\log_{10}$-scale (<0.00000001 kg/s) at LW-1, LW-3, and LW4. The maximum brine leakage rates to Aquifer 1 across LW-1, LW-2, LW-3, and LW-4 (−5.1, −4.2, −4.9, and −4.7, respectively, on a $\log_{10}$-scale) varied by up to almost an order-of-magnitude, and the maximum brine leakage rates to Aquifer 2 across LW-1, LW-2, LW-3, and LW-4 (−6.6, −5.4, −7.0, and −6.6, respectively, on a $\log_{10}$-scale) varied by up to 1.6 orders-of-magnitude. Unlike the maximum CO_2 leakage rates, which were largely a function of proximity to the CO_2 plume, the brine leakage rates reflect additional factors related to pressure buildup in the storage reservoir (See next section).

At LW-19, the maximum simulated brine leakage rates to Aquifer 1 and Aquifer 2 were −4.3 and −7.1, respectively, on a $\log_{10}$-scale (0.000050 and 0.00000008 kg/s, respectively). The median brine leakage rates were more than an order-of-magnitude lower than the maximum and were

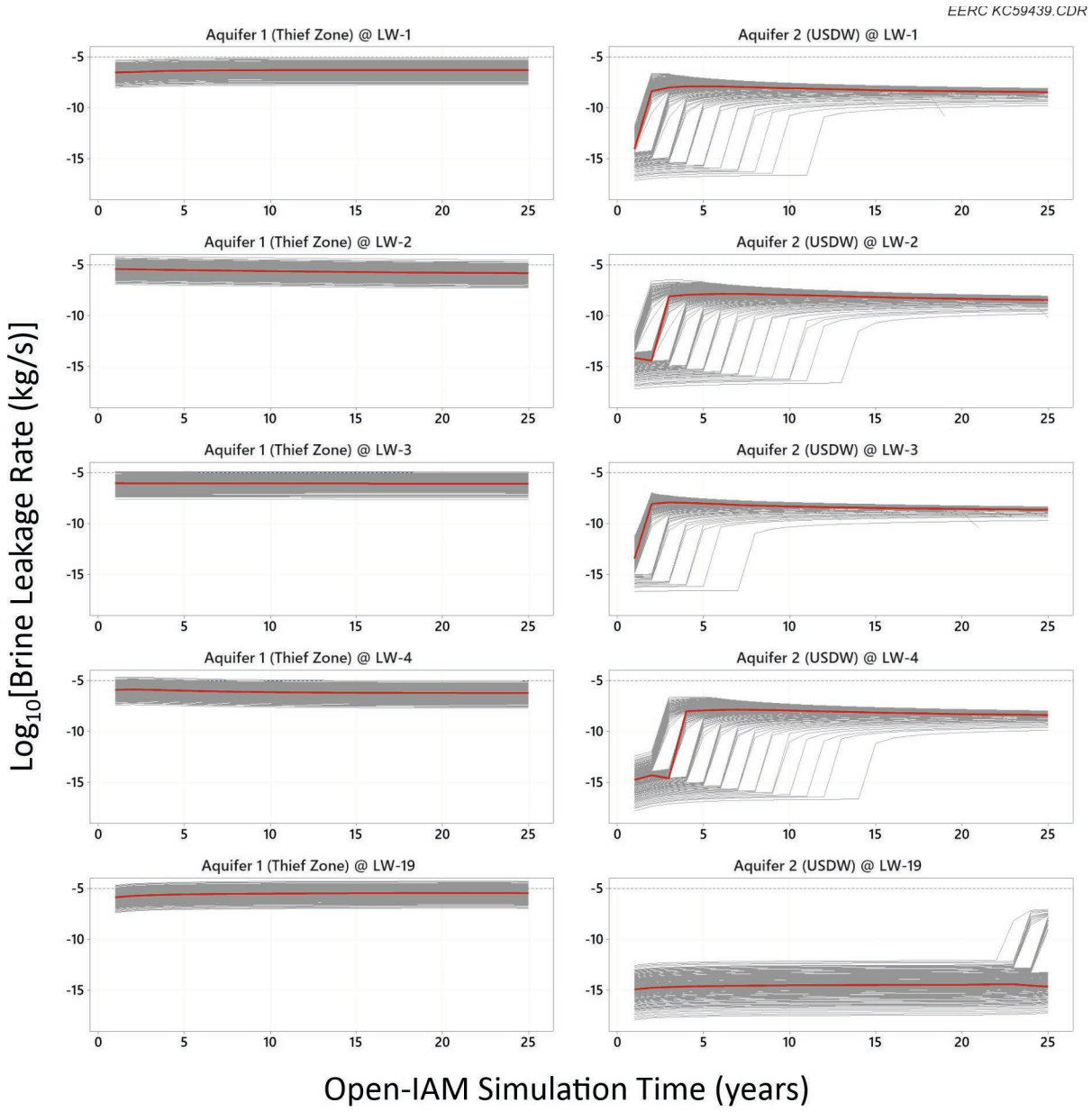

Figure 19. Open-IAM simulated brine leakage rates from the storage reservoir into Aquifer 1 (Thief zone; left column) and Aquifer 2 (USDW; right column) at LW-1, LW-2, LW-3, LW-4, and LW-19. The gray lines show each of the 100 realizations, and the red lines show a LOWESS smoother using a span width of 10%. Blue reference horizontal lines at y = −5 (0.00005 kg/s) have been added to each panel to aid visualization (note: the *y*-axis is on a $\log_{10}$-scale; therefore, zero values are not plotted).

−5.4 and less than −7.0, respectively, on a $\log_{10}$-scale (0.00000354 and <0.00000001 kg/s, respectively). Arrival of brine leakage at Aquifer 2 did not occur until approximately 21 years into the injection operation.

The brine leakage rates show the significant impact of the thief zone, which reduces the brine leakage to the USDW. For example, the maximum brine leakage rates into Aquifer 1 (thief zone) at LW-2 and LW-3 were approximately −4.2 and −4.9, respectively, on a $\log_{10}$-scale (0.000068 and 0.000012 kg/s, respectively), more than an order-of-magnitude higher than the maximum brine leakage rates to Aquifer 2 (USDW) at LW-2 and LW-3. The thief zone phenomenon was described by Nordbotten et al. (2004) as an "elevator model," by analogy with an elevator full of people on the ground floor, who then get off at various floors as the elevator moves up, such that only very few people ride all the way to the top floor.

Brine Leakage Rates with Distance from the Injection Wells

As noted in the Multisegmented Wellbore Component section, the MSW Component uses a one-dimensional multiphase version of Darcy's law to represent flow along a leaky well. Equation 1 provides a simple form of Darcy's law (modified versions of Darcy's law applied to wellbore leakage may be found in Klose et al., 2021).

$$Q = k_{eff} A \frac{\psi_L - \psi_T}{L} \quad \text{[Eq. 1]}$$

Where:

Q is the volumetric flow rate
k_{eff} is the effective permeability of the leaky wellbore
A is the cross-sectional area of flow (related to the wellbore diameter)
ψ_L is the hydraulic potential at the leak-path source (storage reservoir)
ψ_T is the hydraulic potential at the leak-path top (Aquifer 1 or Aquifer 2)
L is the leak length (the length of the wellbore)

Therefore, for a scenario with one effective permeability, cross-sectional area of flow, and leak length, the brine leakage rate is a function of the hydraulic potential difference between the storage reservoir and the aquifer ($\psi_L - \psi_T$). A proxy for the hydraulic potential difference between the storage reservoir and the aquifer is pressure buildup in the storage reservoir since pressure in the aquifer remains relatively constant.

LW-1, LW-2, LW-3, and LW-4 were colocated with the injection wells. The other leaky wellbores were located farther from the four injection wells, ranging from 2 to 17 km from the centroid of the four injection wells. As shown in Section 3.1.5, the pressure buildup around the four injection wells radiates outward in a near-circular pattern caused by the combined effects of CO_2 injection at IW-1, IW-2, IW-3, and IW-4 (overlapping pressure fronts or pressure interference). This pressure buildup pattern from Section 3.1.5 (Figure 11) is repeated in Figure 20. Leaky wellbores located near the centroid of the four injection wells (LW-17, LW-18, and LW-19) experienced the highest pressure buildup (dark gray area), while leaky wellbores located near the perimeter of the model domain and farthest from the injectors (LW-5, LW-10, and LW-12) experienced the least pressure buildup (light gray areas).

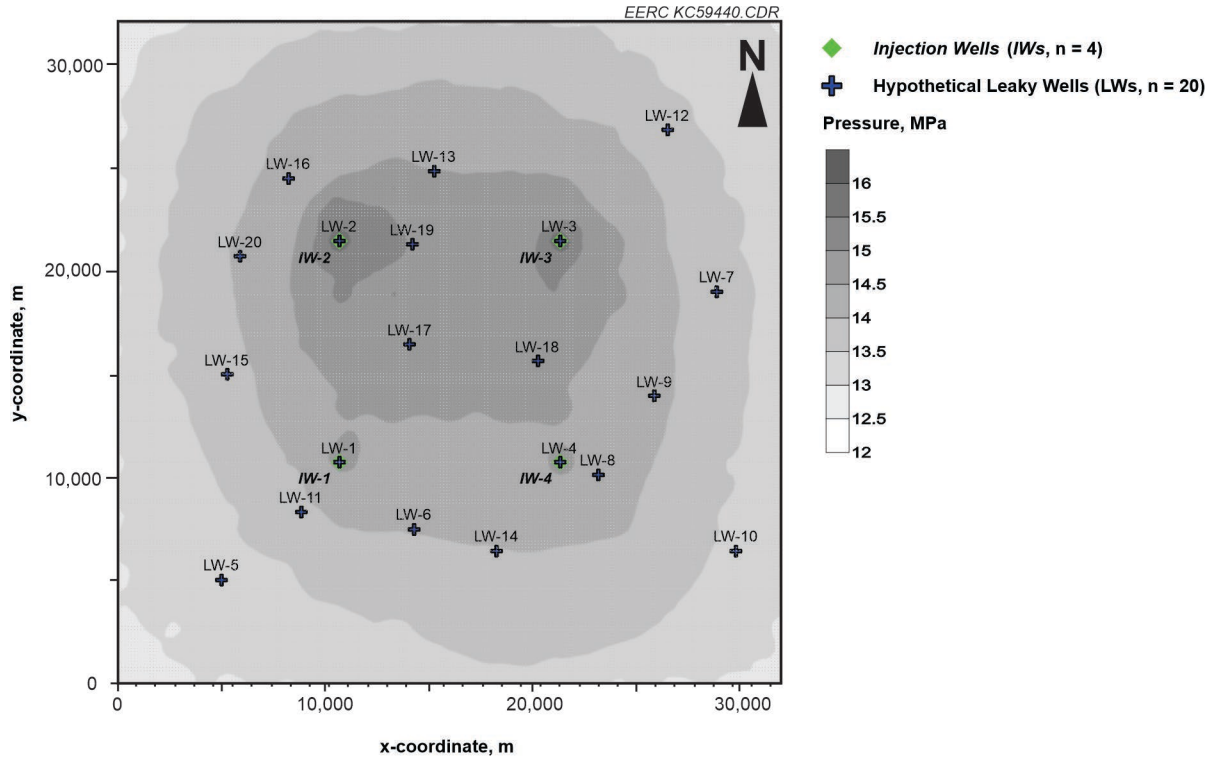

Figure 20. Map showing the Open-IAM study site (211 × 211 grid cells) with pressure at the end of the 25-year CO_2 injection period and the locations of four injection wells (IW-1 to IW-4) and twenty hypothetical leaky wells (LW-1 to LW-20) used in the Open-IAM testing.

Figure 21 shows the brine leakage rates over the 25-year injection period to Aquifer 1 (Thief zone – bottom panel) and Aquifer 2 (USDW – top panel) for Leaky Wellbores LW-17, LW-18, and LW-19 (near group), as compared to leaky wellbores LW-5, LW-10, and LW-12 (far group). As shown in the figure, the brine leakage rates to Aquifer 1 were about a 0.3 (on a $\log_{10}$-scale – roughly a factor of two) greater for the leaky wellbores LW-17, LW-18, and LW-19 closest to the centroid of the injection wells. For example, the average brine leakage rate for the near group wells was approximately –5.5 on a $\log_{10}$-scale (3.2E-06 kg/s); however, the average brine leakage rate for the far group wells was closer to –5.8 on a $\log_{10}$-scale (1.6E-06 kg/s) (bottom panel of Figure 21). The pressure buildup in the storage reservoir was insufficient to raise brine up the leaky wellbores, past Aquifer 1 and into Aquifer 2. The average brine leakage rates to Aquifer 2 were nearly nine orders-of-magnitude lower than the average brine leakage rates to Aquifer 1 and were essentially zero, i.e., less than −14.5 on a $\log_{10}$-scale (3.1E-15 kg/s), and likely reflect numerical values in the analytical solutions that have no environmental relevance. Therefore, the Open-IAM results show that i) leaky wellbores located farther from the injection wells pose a lower leakage impact risk, which could be used to define a threshold area beyond which no leakage impact occurs and ii) the presence of a thief zone between the storage reservoir and the USDW significantly diminishes the potential for brine leakage reaching the USDW.

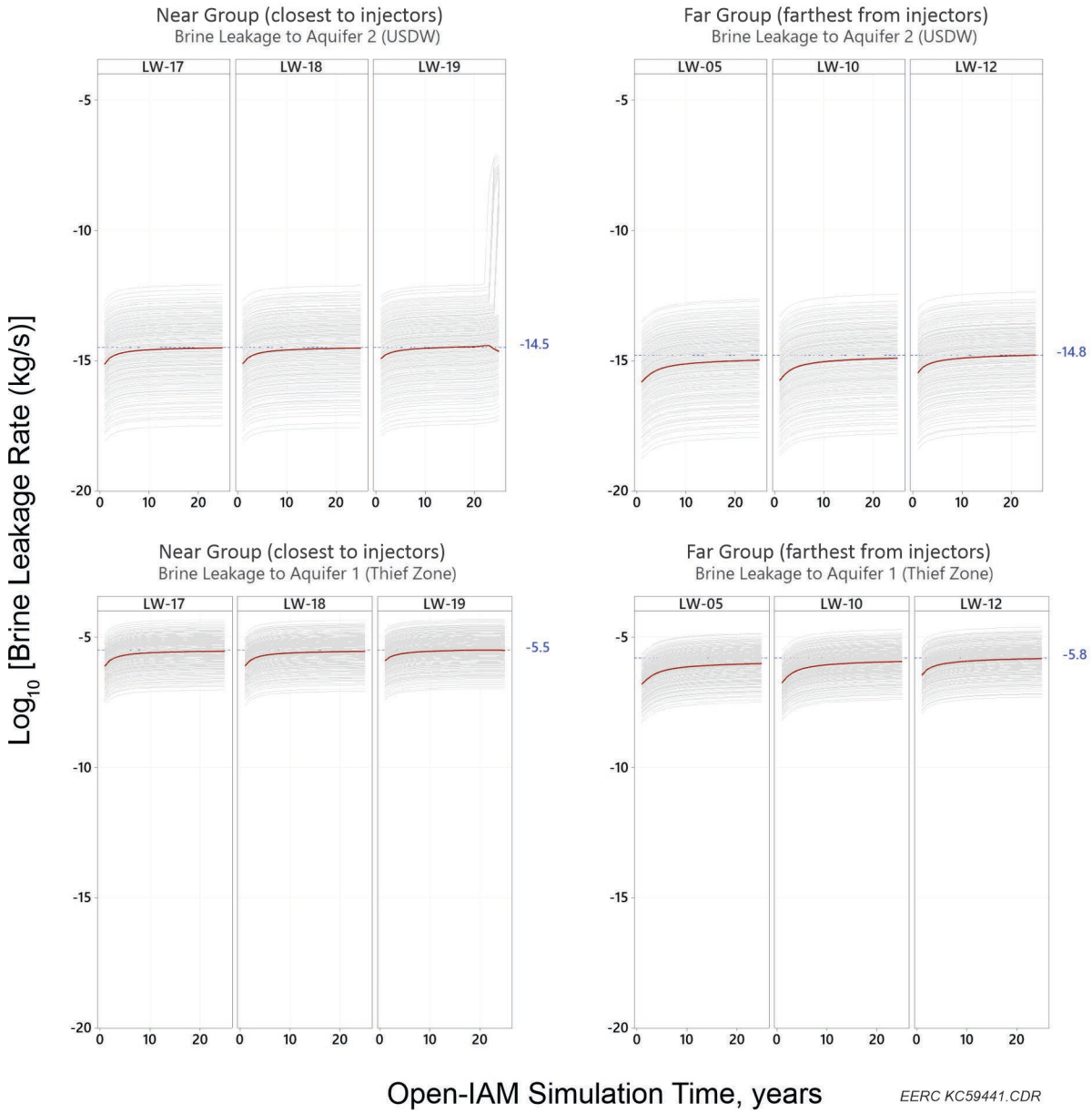

Figure 21. Open-IAM simulated brine leakage rates from the storage reservoir into Aquifer 2 (USDW – top panel) and Aquifer 1 (Thief zone – bottom panel) at the three leaky wellbores located closest to the centroid of the four injection wells (near group: LW-17, LW-18, and LW-19 [left]) compared to the three leaky wellbores located farthest from the centroid of the four injection wells (far group: LW-05, LW-10, and LW-12 [right]) The gray lines show each of the 100 realizations, and the red lines show a LOWESS smoother using a span width of 10%. Blue reference lines have been added to the panels to aid visualization (note: the *y*-axis is on a $\log_{10}$-scale).

Cumulative CO_2 Mass Leakage into Aquifer 1 and Aquifer 2

Figure 22 shows the time-series of cumulative CO_2 mass leakage in metric tons (tonnes) from the storage reservoir into Aquifer 1 (Thief zone) and Aquifer 2 (USDW) at LW-1, LW-2, LW-3, LW-4, and LW-19 over the 25-year injection period. The cumulative CO_2 mass leakage into Aquifer 1 is approximately an order-of-magnitude larger than that of Aquifer 2. The maximum cumulative CO_2 mass leakage into Aquifer 1 and Aquifer 2 was at LW-3 and was 2431 and 178 tonnes, respectively. The cumulative CO_2 mass leakage into Aquifer 1 at LW-1, LW-2, LW-4, and LW-19 was 1143, 1095, 758, and 2 tonnes, respectively, and the cumulative CO_2 mass leakage into Aquifer 2 at these locations was 171, 168, 154, and 1 tonnes, respectively. As previously discussed, the CO_2 leakage rates at all other wells located beyond the CO_2 plume were zero; therefore, the cumulative CO_2 mass leakage into Aquifer 1 and Aquifer 2 from the other leaky wellbores was zero. The cumulative CO_2 mass leakage estimates provide useful inputs for assessing potential CO_2 impacts to the USDW should leakage occur through one or more leaky wellbores.

Impact Plumes: TDS, Pressure, pH, and Dissolved CO_2 Plume Diameter

The FutureGen 2.0 AZMI Component (used for Aquifer 1 – thief zone) and the FutureGen 2.0 Aquifer Component (used for Aquifer 2 – USDW) estimate four variables that could act as proxy measurements for the physical and chemical impacts to Aquifer 1 (thief zone) and Aquifer 2 (USDW) caused by the brine and CO_2 leakage from the leaky wellbores: TDS (total dissolved solid), pressure, pH, and dissolved CO_2 (note: temperature was not included from the FutureGen 2.0 AZMI Component but was part of the FutureGen 2.0 Aquifer Component). These components estimate the dimensions in the *x*- (length), *y*- (width), and *z*-direction (height) (m: dx/dy/dz) of the change in these four measurements around each leaky wellbore (impact plumes). Figures 23, 24, 25, and 26 show the estimated diameters of change in TDS, pressure, pH, and dissolved CO_2, respectively, around LW-1, LW-2, LW-3, LW-4, and LW-19 over 25 years of injection period.

The diameters of TDS changes around the leaky wellbores were relatively small and only extended a few meters in Aquifer 1. The maximum TDS plume diameters observed in Aquifer 1 around LW-2 and LW-19 and were 5.1 m and 5.0 m, respectively. The TDS plume diameters in Aquifer 2 were considerably smaller, less than a meter at all the leaky wells (Figure 23). These results suggest that monitoring for brine leakage by measuring TDS would need to sample within five meters (or less) of the leaky wellbore to detect a change from baseline conditions at these leakage rates.

The diameters of pressure changes around the leaky wellbores were very small and were less than 1.5 m in Aquifer 1 and almost nonexistent (less than half a meter) in Aquifer 2 (Figure 24).

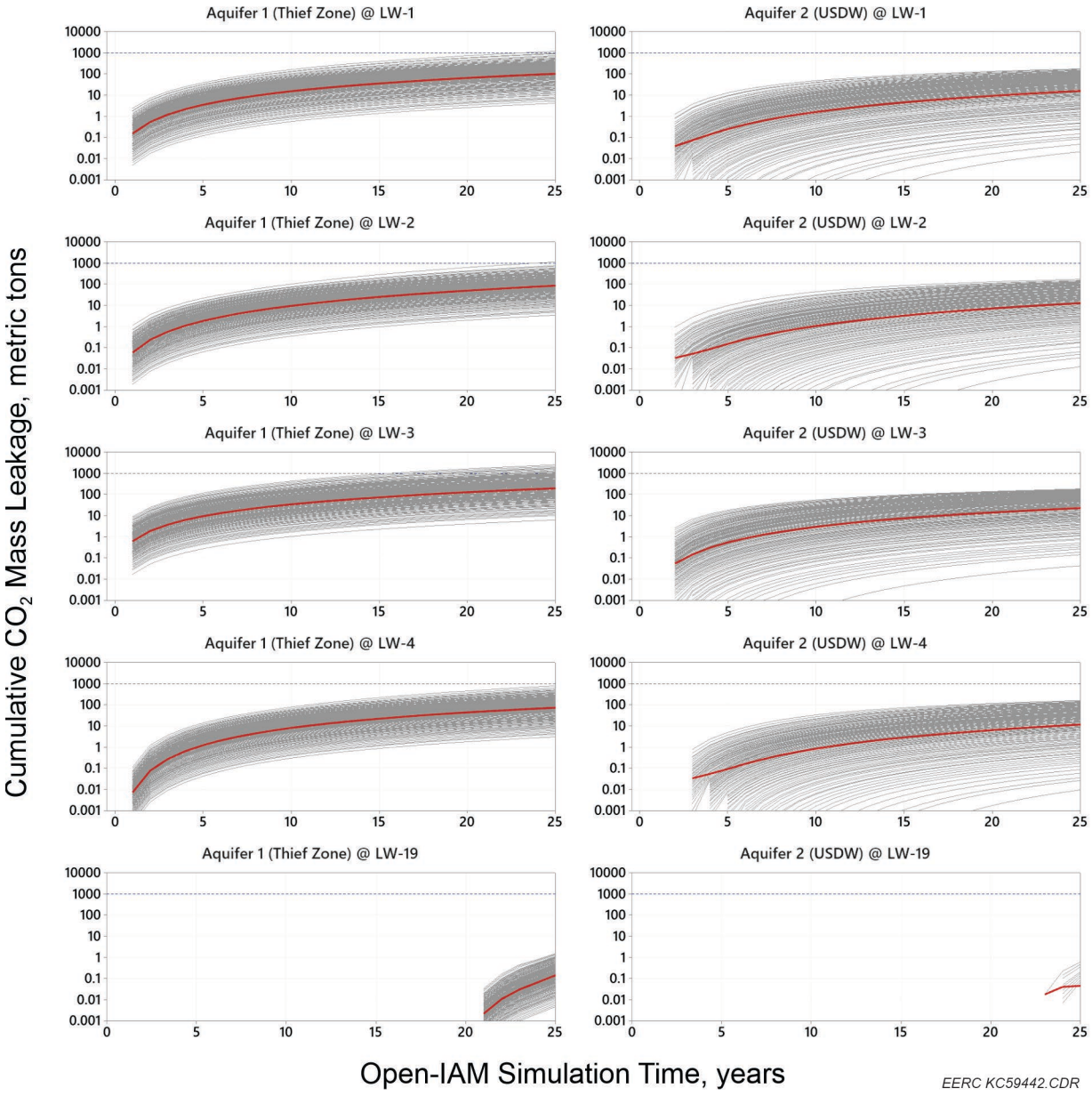

Figure 22. Cumulative CO_2 mass leakage (metric tons, *y*-axis) from the storage reservoir into Aquifer 1 (Thief zone; left column) and Aquifer 2 (USDW; right column) at LW-1, LW-2, LW-3, LW-4, and LW-19. The gray lines show each of the 100 realizations, and the red lines show a LOWESS smoother using a span width of 10%. Blue reference lines have been added to the panels at 1000 metric tons to aid visualization (note: the *y*-axis is on a $\log_{10}$-scale).

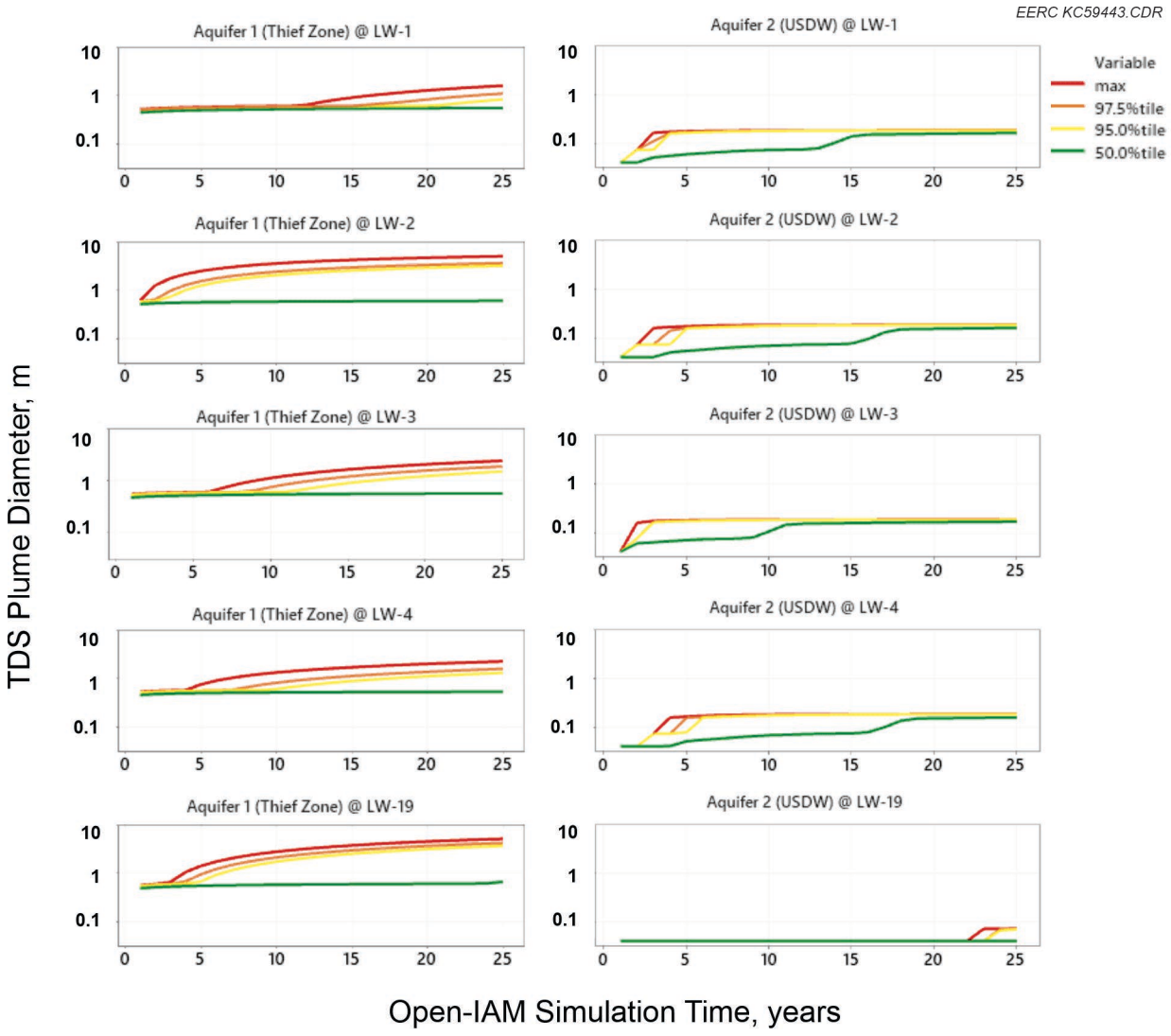

Figure 23. Maximum, 97.5th, 95th, and 50th percentile diameters of measurable TDS changes in Aquifer 1 (thief zone, left panel) and Aquifer 2 (USDW, right panel) around LW-1, LW-2, LW-3, LW4, and LW-19 (note: the *y*-axis is on a $\log_{10}$-scale).

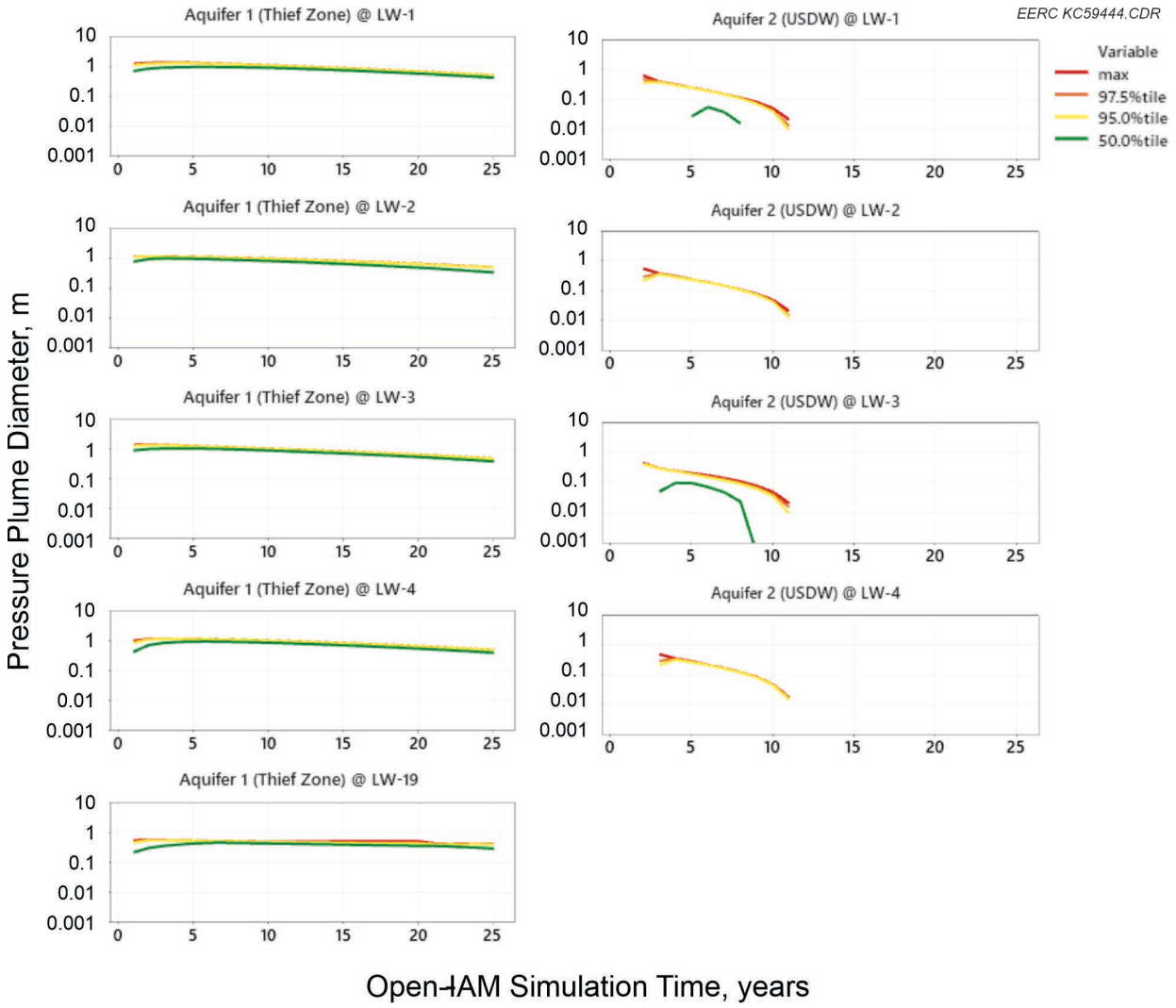

Figure 24. Maximum, 97.5th, 95th, and 50th percentile diameters of measurable pressure changes in the Aquifer 1 (thief zone, left panel) and Aquifer 2 (USDW, right panel) around the LW-1, LW-2, LW-3, LW4, and LW-19 (note: the *y*-axis is on a $\log_{10}$-scale).

The diameters of pH changes around the leaky wellbores were considerably larger, up to 51.0 m (LW-1) and 50.6 m (LW-2) in Aquifer 1. In Aquifer 2, diameters of pH changes around the leaky wellbores were less than 10 meters. Arrival of the pH plume in Aquifer 1 and Aquifer 2 at LW-19 did not occur until approximately 21 and 23 years, respectively, during the injection operation (Figure 25). The maximum pH plume diameter observed in the Aquifer 1 and Aquifer 2 at LW-19 was 12.1 and 3.6 m, respectively.

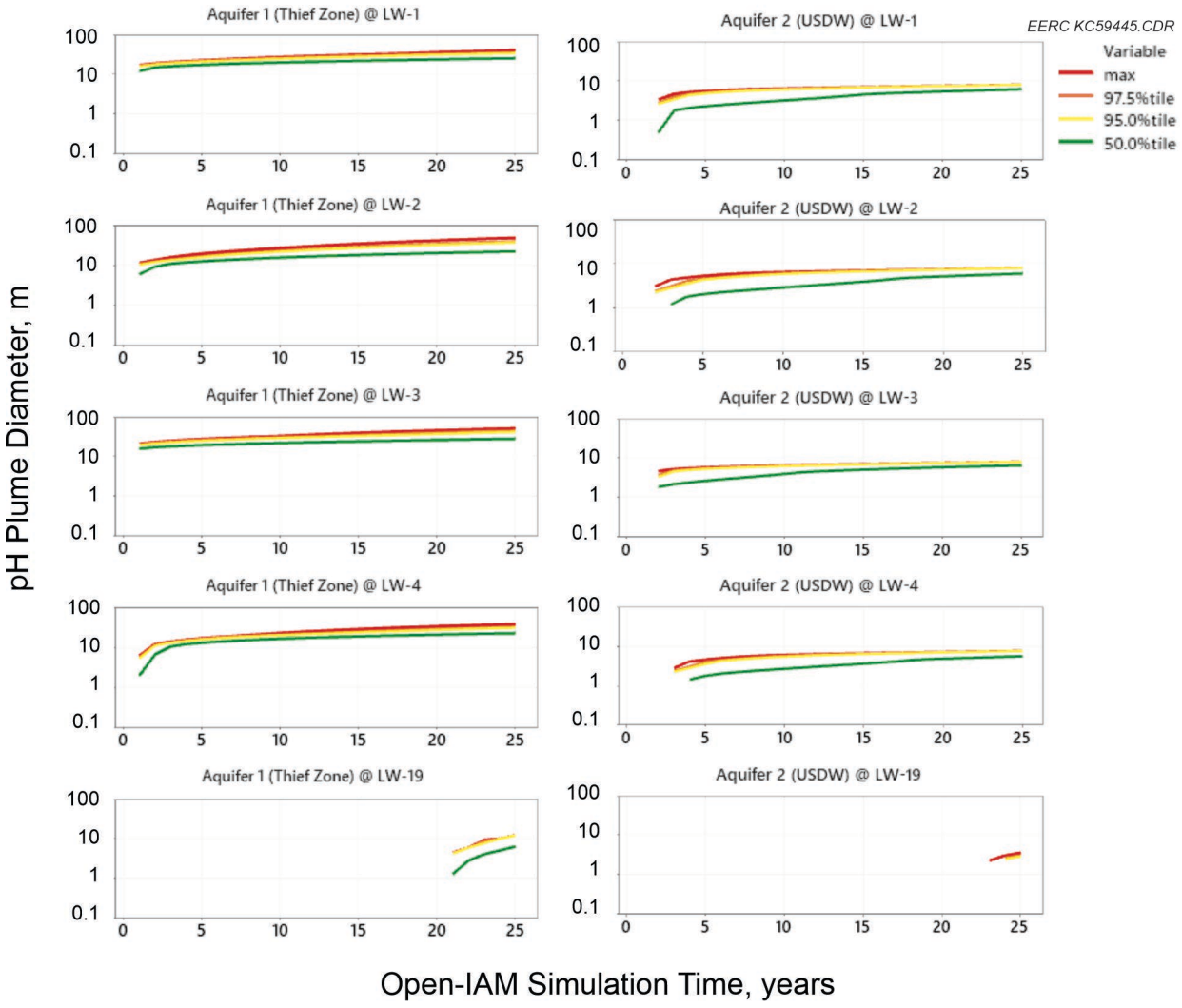

Figure 25. Maximum, 97.5th, 95th, and 50th percentile diameters of measurable pH changes in the Aquifer 1 (thief zone, left panel) and Aquifer 2 (USDW, right panel) around the LW-1, LW-2, LW-3, LW4, and LW-19 (note: the *y*-axis is on a $\log_{10}$-scale).

The diameters of dissolved CO_2 changes around the leaky wellbores were similar in magnitude to those for pH in both Aquifer 1 and Aquifer 2. The maximum dissolved CO_2 plume diameters observed in the Aquifer 1 were 51.5 m (LW-1) and 51.6 m (LW-2). In Aquifer 2, diameters of dissolved CO_2 changes were less than 30 meters. Arrival of the dissolved CO_2 plume in the Aquifer 1 and Aquifer 2 at LW-19 did not occur until approximately 21 and 23 years, respectively, during the injection operation (Figure 26). The maximum dissolved CO_2 plume diameters observed in the Aquifer 1 and Aquifer 2 at LW-19 were 17.2 and 13.5 m, respectively.

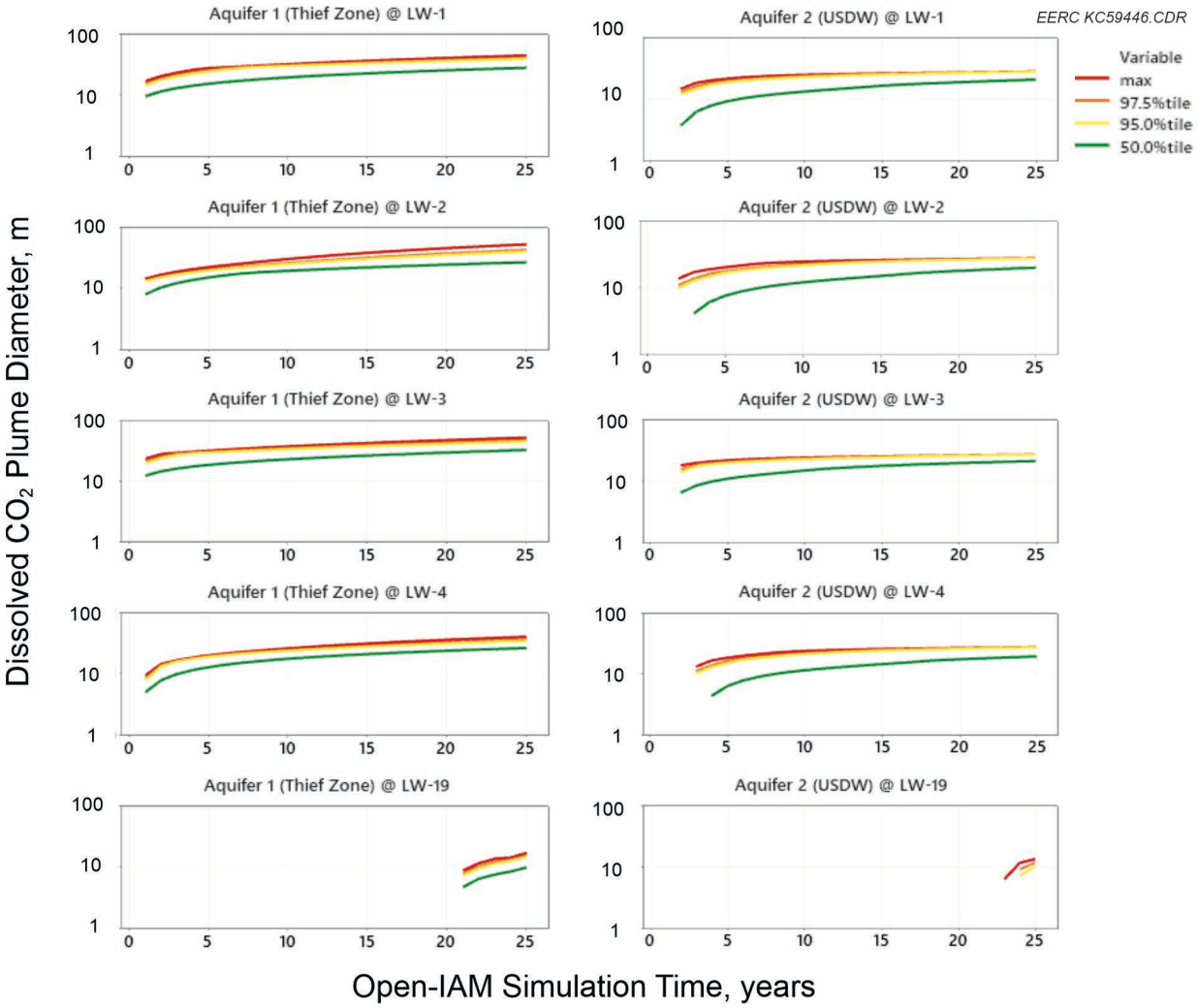

Figure 26. Maximum, 97.5th, 95th, and 50th percentile diameters of measurable dissolved CO_2 changes in the Aquifer 1 (thief zone, left panel) and Aquifer 2 (USDW, right panel) around the LW-1, LW-2, LW-3, LW4, and LW-19 (note: the *y*-axis is on a $\log_{10}$-scale).

Probability Maps of Dissolved CO_2

The preceding figures showing each of the 100 realizations provide useful information about the potential CO_2 and brine leakage through the leaky wellbores and the variability (uncertainty) in those estimates attributable to the user-defined uncertainty in the leaky wellbore effective permeability – three orders-of-magnitude from 10^{-13} to 10^{-16} m^2 (with a mode of 10^{-14} m^2). These outputs can be extended to estimate the probability of a leakage event of a given magnitude, which could provide useful information to storage project risk management decision-making. This section illustrates example "probability maps," which show the probability of the dissolved CO_2 impact plume diameter exceeding a given threshold diameter around the leaky wellbores colocated with the injection wells: LW-1, LW-2, LW-3, and LW-4. The calculation of probability used a "frequentist" approach and the FutureGen 2.0 AZMI Component outputs for Aquifer 1 (thief zone)

and the FutureGen 2.0 Aquifer Component outputs for Aquifer 2 (USDW). The calculation approach first defined an arbitrary threshold diameter and then counted the number of realizations that met or exceeded that threshold at the end of the 25-year injection period, dividing by 100 to express the outcome as a fraction in the unit interval 0–1. For example, if 100 of 100 realizations exceeded a dissolved CO_2 impact plume diameter greater than or equal to 2 m, then the probability was 100% (1.0). However, if only 50 of 100 realizations exceeded a dissolved CO_2 impact plume diameter greater than or equal to 10 m, then the probability was only 50% (0.50). Several threshold diameters were used to create contour maps of the probability for each aquifer and well.

Figure 27 shows the probability maps for the dissolved CO_2 impact plume diameters in Aquifer 1 and Aquifer 2 around LW-1. The diameters of the circles with greater than 90% probability (red/dark orange) in Aquifer 1 and Aquifer 2 are roughly 20 and 10 m, respectively (the grid spacing in Figures 27–30 is 10 meters). However, the diameters of the circles with greater than 1% probability in Aquifer 1 and Aquifer 2 are roughly between 50 and 30 m, respectively. The results for the other leaky wellbores LW-2 (Figure 28), LW-3 (Figure 29), and LW-4 (Figure 30) were similar.

The probability maps provide visualizations to help inform decision-making about the likelihood of exceeding an impact plume diameter of a given size as well as the design of a monitoring plan for detecting changes from baseline conditions.

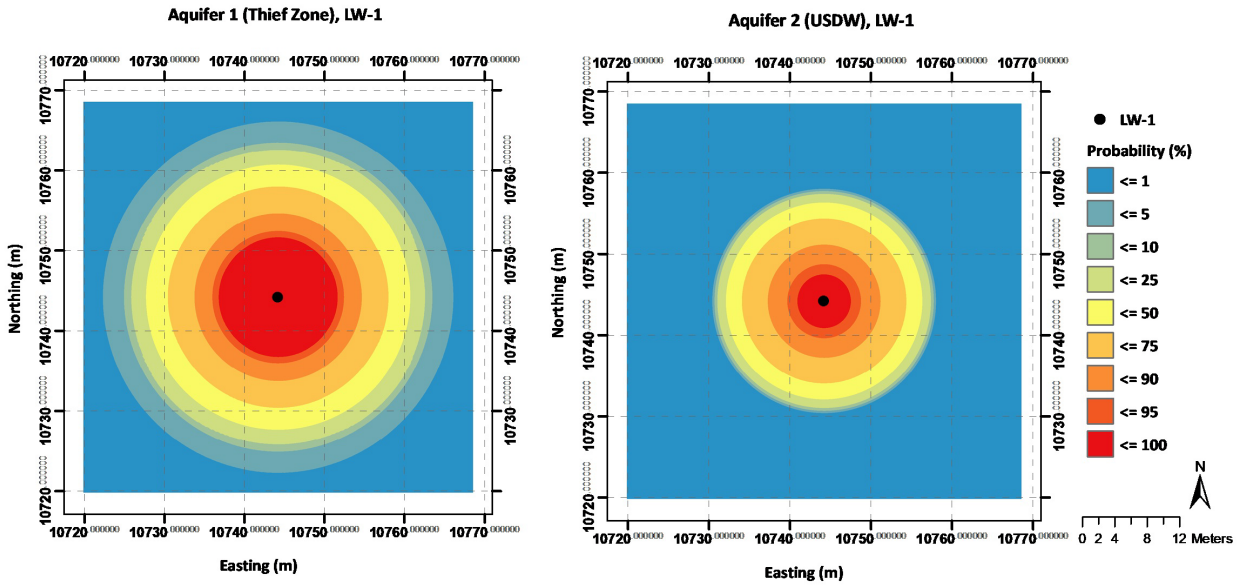

Figure 27. Probability map of the dissolved CO_2 impact plume diameter around LW-1 in Aquifer 1 (Thief zone, left panel) and Aquifer 2 (USDW, right panel) based on 100 realizations with varying leaky wellbore effective permeability inputs. The grid interval in both panels is 10 meters.

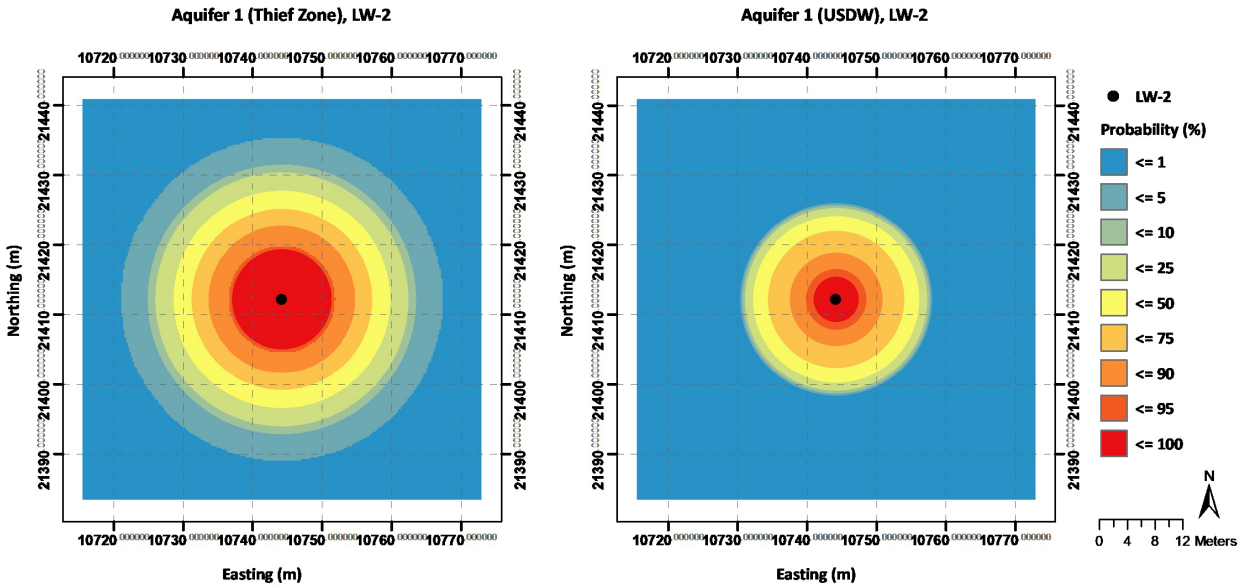

Figure 28. Probability map of the dissolved CO_2 impact plume diameter around LW-2 in Aquifer 1 (thief zone, left panel) and Aquifer 2 (USDW, right panel) based on 100 realizations with varying leaky wellbore effective permeability inputs. The grid interval in both panels is 10 meters.

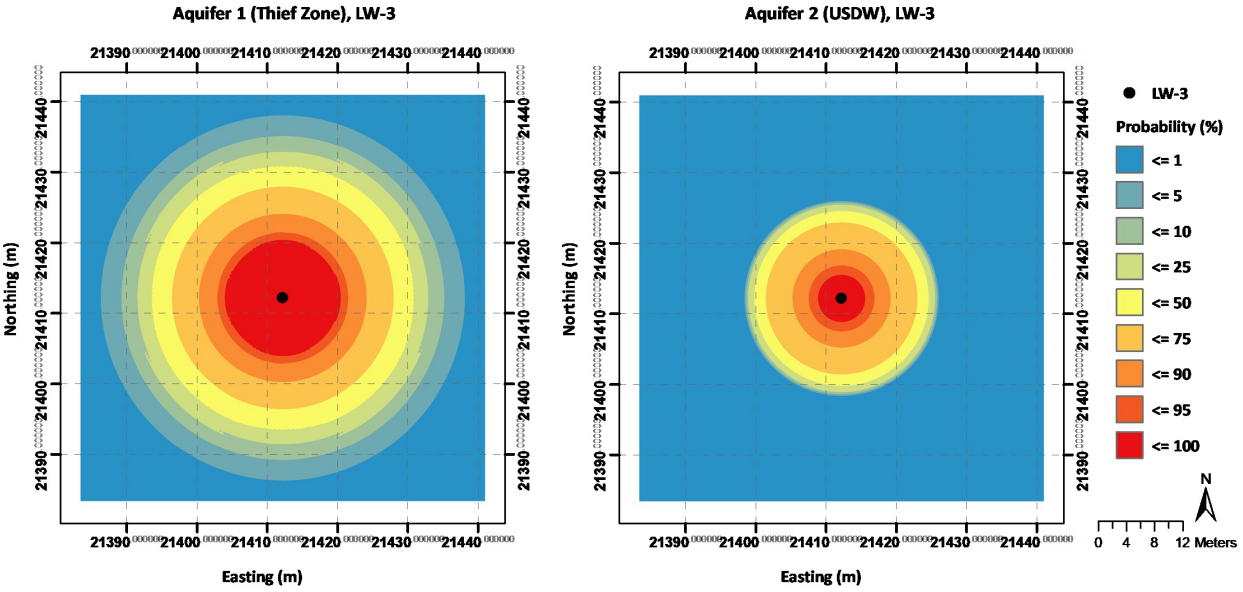

Figure 29. Probability map of the dissolved CO_2 impact plume diameter around LW-3 in Aquifer 1 (thief zone, left panel) and Aquifer 2 (USDW, right panel) based on 100 realizations with varying leaky wellbore effective permeability inputs. The grid interval in both panels is 10 meters.

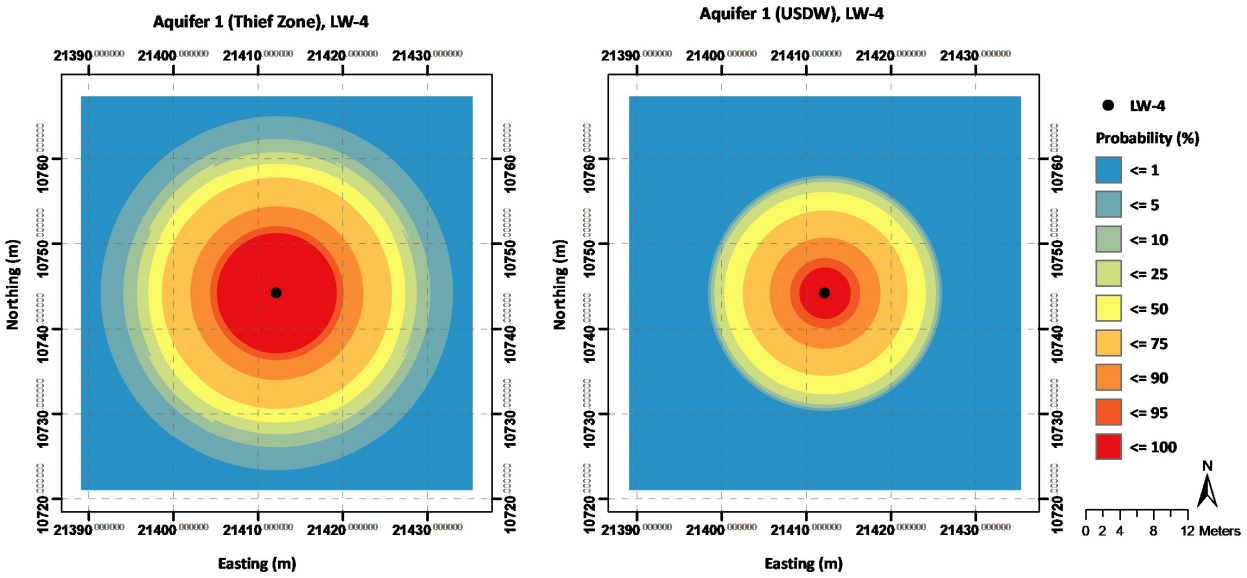

Figure 30. Probability map of the dissolved CO_2 impact plume diameter around LW-4 in Aquifer 1 (thief zone, left panel) and Aquifer 2 (USDW, right panel) based on 100 realizations with varying leaky wellbore effective permeability inputs. The grid interval in both panels is 10 meters.

Assessment

The NRAP tools were subjected to extensive review and iterative refinement during their development. One of the criteria used in assuring the quality of the tools was to develop scientifically credible and technically defensible system component characterizations and an integrated system model. The Open-IAM and its predecessors, NRAP-IAM-CS (Stauffer et al., 2016) and CO_2-PENS (Stauffer et al., 2009), as well as the incorporation of components (ROMs) into the IAM, were all subjected to an NRAP quality assurance review (Dilmore et al., 2016).

The example explored herein is one case in a broad array of potential injection scenarios for a storage project. There is currently no way to validate the Open-IAM results against field data, as the simulations are forecasts about the future (forward-modeling) and there has been no injection or associated monitoring at a storage site to validate the forward-models. However, as illustrated below, the Open-IAM results demonstrate consilience with fundamental physical principles, which provides greater confidence in the results. For example:

1. The Open-IAM simulated reservoir pressure and CO_2 saturation at each wellbore *x*- and *y*-coordinate agreed with the CMG GEM data (processed through Petrel and Python script), which indicates that the LUT Reservoir Component interpolations were accurate and that the handoff from CMG GEM to Open-IAM executed correctly (Figure 16).

2. Leaky wellbores colocated with the injection wells (LW-1, LW-2, LW-3, and LW-4) had the greatest CO_2 leakage rates (Figure 18) and brine leakage rates (Figure 19), which is

consistent with their proximity to the highest pressure buildup and CO_2 saturation in the storage reservoir.

3. The time-series relationship in the simulated leakage rates at LW-1, LW-2, LW-3, and LW-4 were consistent with their spatial relationship to the CO_2 plume and pressure buildup plume; i.e., CO_2 and brine arrived instantaneously in Year 1 at LW-1, LW-2, LW-3, and LW-4, which were located at the injection wells, and arrived much later at LW-19, which was located 2.5 miles east of the Injection Well IW-2 (CO_2 and brine arrived in approximately Year 21).

4. Leaky wellbores located further from the injection well, where there was minimal pressure buildup in the storage reservoir above hydrostatic conditions, had essentially zero brine leakage to Aquifer 2 (USDW), which is consistent with the small hydraulic potential gradient between the storage reservoir and the USDW and the leaky wellbores being open to the Aquifer 1 (thief zone).

5. Brine leakage rates in Aquifer 2 (USDW) observed at the leaky wellbores outside the CO_2 plume area (LW-5 through LW-18, LW-20) show near-zero rates that likely reflect no environmental impact.

6. The cumulative CO_2 mass leakage into Aquifer 1 (thief zone) was larger than the CO_2 mass leaked into the Aquifer 2 (USDW) and was consistent with the time-series CO_2 leakage rates from the storage reservoir into Aquifer 1 and Aquifer 2 at LW-1, LW-2, LW-3, LW-4, and LW-19.

7. Impact plume diameters of four monitoring metrics (TDS, pressure, pH, and dissolved CO_2) were proportional to the leakage rates observed for the different leaky wellbores.

In aggregate, the Open-IAM testing suggests that the tool provides a useful approach for quantifying the impacts of CO_2 and brine leakage from the storage reservoir to overlying aquifers through one or more leaky wellbores located within the storage complex.

KEY FINDINGS

The Open-IAM testing generated the following list of key findings:

1. The example case studies provided by NRAP with the Open-IAM tool and user guide provide helpful guidelines to familiarize the user with Open-IAM's functionality and expected outcomes.

2. In the Stratigraphy Component, the default setting for the number of shale layers is three, which requires two aquifers. A storage complex with less than three shale layers and two aquifers cannot be simulated in the current Open-IAM version. However, the remaining features of the Stratigraphy Component allow the user to create a site-specific storage complex by specifying each geologic unit and thickness.

3. Coupling numerical reservoir simulation outputs for pressure and CO_2 saturation, for example from CMG GEM, with Open-IAM requires that the outputs be formatted to specific Open-IAM specifications for the LUT Reservoir Component. However, the standard formats of CMG GEM export files are not compatible with the input format for the current version of Open-IAM. Consequently, the CMG GEM output needed to be converted into a compatible Open-IAM .csv input file. A Python script was written to reformat the CMG GEM output files into the appropriate.csv file format for the LUT Component. Since most storage project simulations are conducted using a numerical reservoir simulator, exporting results from a numerical reservoir simulator to Open-IAM is a critical first step toward using Open-IAM.

4. When using the MSW Component, the *x*- and *y*-coordinates for the leaky wellbores must be precisely the same as in the input files (i.e., to the same level of numerical precision [decimal places]). Otherwise, the pressure and CO_2 saturation will be calculated based on other interpolation methods.

5. In the MSW Component, each realization specifies a unique value of aquifer permeability over the full wellbore length. The MSW Component does not allow the user to assign distinct permeability values for each aquifer unit. For example, if the thief zone and USDW had different aquifer permeability values, then the MSW Component would not permit the user to assign different permeability values to each of these units.

6. The FutureGen 2.0 AZMI Component and FutureGen 2.0 Aquifer Component provide useful tools for estimating impact plumes of TDS, pressure, pH, and dissolved CO_2 within aquifers. However, while the dimensions in the *x*- (length, dx) and *y*- (width, dy) directions seemed plausible, the *z*-direction (height, dz) of the impact plumes were often erroneous, with heights that exceeded the aquifer thickness. Therefore, postprocessing the FutureGen 2.0 AZMI Component and FutureGen 2.0 Aquifer Component results must truncate the impact plume heights to the aquifer height.

7. The LHS (Latin Hypercube Sampling) can be a useful approach to explore the possible outcome of CO_2 and brine leakage scenarios using stochastic simulations with multiple realizations. The LHS feature provides a useful tool for quantifying uncertainty given sparse site characterization data for storage projects and the associated uncertainty in the storage complex petrophysical properties or the leaky wellbore characteristics.

8. Successfully executing an Open-IAM simulation creates two output text files (*lhs_results.txt* and *lhs_statistics.txt*), which allow the user to visualize the results and to explore the sensitivity of the outputs to the different input parameters.

9. Postprocessing outside of Open-IAM was necessary to properly visualize and assess the Open-IAM simulation results. The built-in postprocessing tools within Open-IAM provide limited ability for combining figure panels, modifying axes, or making other adjustments to enhance the visualizations of the outputs. However, the output files (*lhs_results.txt* and *lhs_statistics.txt* files) were easily amenable to third-party software.

10. The current version of Open-IAM provides a useful tool for heuristic modeling of a storage project and what-if scenario modeling for CO_2 and brine leakage through wellbores. However, the current tool requires significant experience with the Open-IAM GUI and component modules and may not be appropriate for a nonexpert. Improvements in the ability to transfer simulations more easily from CMG GEM to Open-IAM and the GUI input fields would broaden the usability of Open-IAM to a wider set of potential users, for example, regulatory stakeholders.

REFERENCES

Canadian Standards Association, 2012, Z741-12 – geological storage of carbon dioxide.

Carey, J.W., 2017, Probability distributions for effective permeability of potentially leaking wells at CO_2 sequestration sites: NRAPTRS-III-021-2017, NRAP Technical Report Series, U.S. Department of Energy National Energy Technology Laboratory, Morgantown, West Virginia, 28 p.

Celia, M.A., Nordbotten, J.M., Court, B., Dobossy, M., and Bachu, S., 2011, Field-scale application of a semi-analytical model for estimation of CO_2 and brine leakage along old wells: International Journal of Greenhouse Gas Control, v. 5, no. 2, p. 257–269.

Dilmore, R., Wyatt, C., Pawar, R., Carroll, S., Oldenburg, C., Yonkofski, C., Bacon, D., King, S., Lindner, E., Bachmann, C., White, J., Keating, E., Zhang, Y., Bradley, C., Lee, R., Chu, S., Stauffer, P., Huerta, N., and Bromhal, G., 2016, NRAP Phase I tool development and quality assurance process: NRAP-TRS-II-021-2016, NRAP Technical Report Series, U.S. Department of Energy National Energy Technology Laboratory, Morgantown, West Virginia, 64 p.

Fenton, N., and Neil, M., 2013, Risk assessment and decision analysis with Bayesian networks: Boca Raton, Florida, CRC Press.

International Organization for Standardization, 2017, Carbon dioxide capture, transportation, and geological storage — geological storage: ISO 27914:2017-10.

King, S., 2016, Reservoir reduced-order model – generator (RROM-Gen) tool user's manual, version 2016.11-1.2: NRAP-TRS-III-014-2016, NRAP Technical Report Series, U.S. Department of Energy National Energy Technology Laboratory, Morgantown, West Virginia, 16 p.

Klose, T., Chaparro, M.C., Schilling, F., Butscher, C., Klumback, S., and Blum. P., 2021, Fluid flow simulations of a large-scale borehole leakage experiment: Transport in Porous Media, v. 136, p. 125–145. https://doi.org/10.1007/s11242-020-01504-y (accessed November 2021).

Minitab 19 Statistical Software, 2020, Computer software, State College, Pennsylvania, Minitab, Inc. (www.minitab.com).

Nordbotten, J., Celia, M., and Bachu, S., 2004, Analytical solutions for leakage rates through abandoned wells. Water Resources Research, v. 40, no. 4, p. W042041–W0420410. https://doi.org/10.1029/2003WR002997 (accessed November 2021).

Stauffer, P.H., Viswanathan, H.S., Pawar R.J., and Guthrie, G.D., 2009, A system model for geologic sequestration of carbon dioxide: Environmental Science & Technology, v. 43, p. 565–570.

Stauffer, P., Chu, S., Tauxe, C., and Pawar, R., 2016, NRAP integrated assessment model-carbon storage (NRAP-IAM-CS) tool user's manual, Version: 2016.11-1.1, NRAP-TRS-III-010-2016, NRAP Technical Report Series, U.S. Department of Energy National Energy Technology Laboratory, Morgantown, West Virginia, 64 p.

Vasylkivska, V., King, S., Bacon, D., Harp, D., Keating, E., Yang, Y., Zhang, Y., Chen, B., and Mansoor, K., 2021, NRAP-Open-IAM user's guide, release alpha 2.2.0-21.02.12: U.S. Department of Energy National Energy Technology Laboratory, Morgantown, West Virginia.

Vermeul, V.R., Amonette, J.E., Strickland, C.E., Williams, M.D., and Bonneville, A, 2016, An overview of the monitoring program design for the FutureGen 2.0 CO_2 storage site: International Journal of Greenhouse Gas Control, v. 51, p. 193–206.

Yonkofski, C.M., Whiting, J.M., Huang, B.Z., and Hanna, A.C., 2020, Designs for risk evaluation and management (DREAM) tool user's manual, Version 2020.01-2.0: NRAP-TRS-III-001-2020, NRAP Technical Report Series, U.S. Department of Energy National Energy Technology Laboratory, Morgantown, West Virginia, 45 p.